RILUZOLE INDUCES DNA DOUBLE STRAND BREAKS IN MGLUR1 EXPRESSING HUMAN MELANOMA CELLS

By

ROBERT M. CERCHIO JR

A thesis submitted to the

School of Graduate Studies

Rutgers, The State University of New Jersey

In partial fulfillment of the requirements

For the degree of

Master of Science

Graduate Program in Toxicology

Written under the direction of

Suzie Chen

And approved by

_____

_____

_____

New Brunswick, New Jersey

OCTOBER, 2018

ABSTRACT OF THESIS

Riluzole Induces DNA Double Strand Breaks in mGluR1 Expressing Human Melanoma Cells

By ROBERT MICHAEL CERCHIO JR

Thesis Director: Dr. Suzie Chen

Melanoma is the most aggressive form of skin cancer; in 2018 about 90,000 new cases and 9,000 deaths are expected in the United States. Our group described the oncogenic potential of a normal neuronal cell receptor, metabotropic glutamate receptor 1 (mGluR1), when aberrantly expressed in melanocytes, the pigment producing cells. Deregulated melanocytic cell proliferation leads to neoplastic transformation and progression to spontaneous metastatic melanoma in a transgenic mouse model. The natural ligand of mGluR1 is glutamate and it is well known that all cells, particularly cancer cells, depend on glutamine/glutamate for growth. We showed that mGluR1 expressing cells establish autocrine/paracrine loops by secreting glutamate to the extracellular space to ensure constitutive activation of the receptor, mGluR1 and promote cell growth. Treatment of these cells with pharmacological inhibitor of mGluR1 or through genetic manipulation by silencing RNA to reduce the receptor expression, render the receptor nonfunctional and led to cell cycle arrest at the G2/M phase followed by apoptotic cell death. Riluzole is FDA approved for the treatment of

amyotrophic lateral sclerosis (ALS) and one of its functions is the inhibition of glutamate release. This allows the drug to function as an antagonist to mGluR1 activity. Examination of riluzole treated melanoma cells reveals elevated levels of phosphorylated histone H2AX (γH2AX), a protein marker for DNA double-stranded breaks (DSBs). Furthermore, increased ROS levels and decreased intracellular glutathione were also detected in riluzole-treated melanoma cells. We hypothesize that riluzole interacts with the glutamate/cystine antiporter (xCT) to reduce glutamate efflux and cystine influx. Cystine, when reduced to cysteine, is a critical component in glutathione synthesis. Limiting the influx of cystine reduces glutathione levels in the cell, resulting in oxidative DNA damage. The overall goal of this thesis is to determine the consequences of riluzole-induced DNA damage when an ROS scavenger such as N-Acetylcysteine (NAC) is included in the growth media. Effects on DNA damage was assessed using protein markers for single-stranded and double-stranded DNA breaks (SSBs). Alkaline and neutral conditioned COMET assays are used to ascertain the types of riluzole-induced DNA damage. Lastly, by using flow cytometric intracellular staining analysis and guided by the presence of inhibitors to two different DNA repair pathways we were able to conclude that the oxidative damage induced by riluzole is likely DSBs and at Non Homologous End Joining (NHEJ) repair pathway is the preferred double strand break pathway used by mGluR1-expressing melanoma cells.

ACKNOWLEDGEMENTS

The last 3 years as a graduate student has challenged me with a multitude of obstacles, both professional and personal, that helped play a role in shaping the scientist and person I have become. For as long as I can remember, I wanted to be a scientist, but I never truly understood what it meant to be one. I'd like to extend my deepest and greatest gratitude to my advisor, Dr. Suzie Chen, in teaching me the gravity of what being a scientist means. Suzie, I came into your lab a naïve graduate student, but you taught me the how to work thoroughly but efficient, and to always keep asking myself "why am I doing this". Thank you for taking me into your lab and teaching me the valuable work and life lessons I will take with me into my career.

I would also like to thank my committee members; Dr. Helmut Zarbl and Dr. Lori White for helping me complete my graduate studies. Next I would like to thank the members of the Chen lab for their support and the work environment I had throughout grad school. Thank you Christina for your helping hand with some of my experiments, and Raj and Kevinn for providing workplace conversations.

Last but not least I'd like to thank my friends and family. Without you I would not be who and where I am today. Thank you to my mother and father for all the support you have given me throughout my childhood into my young adult life and for encouraging me to never stop being curious. Thank you to my friends who have stuck with me throughout the years and reminding me to have some fun in between work. And thank you Hannah for being so supportive throughout my thesis and being by my side during those times I felt overwhelmed.

TABLE OF COTENTS

Page

List of Figures

INTRODUCTION

A. Cancer

In the year 2018, there will be a predicted 1.7 million new cases and over 600,000 deaths related to cancer in the United States alone (Siegel *et al.* 2018). Cancer is a devastating disease where normal cells experience uncontrolled cell growth and transform into what is referred to as a tumor. The disease can affect multiple different organ systems throughout the body and, as a result, millions of individuals around the globe will develop some form of this debilitating illness each year. Although they all share the characteristic deregulated cell growth, there are additional features that differentiate individual cancers of the same origin from one another. This has made it difficult to develop therapies that treat a broad spectrum of cancer types.

The nomenclature of a cancer describes its tissue of origin. Cancers that classify as carcinoma arise from epithelial tissue and are the most commonly diagnosed cancer type because they can develop in almost all major organs such as breast, pancreas, colon, lungs, and skin. Tumors that arise from nonepithelial tissue, such as smooth muscle, fat, and bone, are referred to as sarcomas; these cancers are not as common as carcinomas, but can be more deadly since they are more difficult to detect at early stages. Lymphomas and leukemia are cancers of lymphocytes and blood respectively and are most common in children. Lastly, melanoma, cancer that arises from transformed melanocytes, the pigment producing cells, is the most dangerous form of skin cancer and accounts for the majority of death from this cancer type. Although many

unique characteristics separate the different types of cancers from one another, they all share the distinctive phenotype of uncontrollable cell growth.

When cells transform, the consequential tumor is described as either benign or malignant. A benign tumor remains localized in its tissue of origin and increases in size where it damages local healthy tissue around it, either through sheer pressure or taking nutrients from healthy cells. A malignant tumor is one that not only grows and invades surrounding tissue, but may also metastasize to distant parts of the body either through the lymphatics or the vascular systems. Once they spread to an organ, malignant tumors interfere with normal organ function by consuming more nutrients than healthy cells to sustain their growth and activity.

B. Melanoma

Melanoma is a highly malignant cancer estimated to comprise for 91,270 new cases and 9,320 deaths in 2018 (Siegel *et al.,* 2018). Risk factors associated with the disease include familial history, sun exposure, immune suppression, and nevi on the skin. Melanoma tumors arise from melanocytes, which are the pigment-producing cells located in the basal layer of the epidermis of the skin. It is possible for a gain of function mutation to occur in melanocytes that allows them to undergo cellular proliferation and form dark spots on the skin called nevi. Generally, most melanocytes in nevi rapidly proliferate until they enter cellular senescence, a state in which cells cease to proliferate. However, additional mutations in DNA may allow some melanocytes to bypass cell checkpoints, transform into malignant melanoma cells, and further progress into a tumor (Ha *et al.*, 2008). Neoplastic transformation of melanocytes into melanoma

can result from a multitude of complications to a cell. The most common and preventable of these is DNA mutations resulting from UV radiation from absorbed sunlight. A specific example of DNA damage induced mutation that can lead to melanoma development is the mutation of protein(s) that regulate cell growth, such as the serine-threonine protein kinase BRAF.

At least three major cell-signaling pathways have been linked to melanoma development: the mitogen-activated protein kinase (MAPK), phosphatidylinositide 3-kinase/AKT (PI3K/AKT), and p16INK4a/p14 signaling pathways. Stimulating the MAPK pathway leads to cellular proliferation; and mutations in proteins within MAPK, such as RAF and RAS, can lead to over activation of the pathway, resulting in continual proliferation. The PI3K/AKT pathway is an anti-apoptotic pathway whose activation increases cell survival; a mutation in proteins in this pathway prevents cells from undergoing apoptosis (Chappell *et al.*, 2011). The third pathway involves p16INK4a and p14 where a loss of function mutation in the tumor suppressor protein, cyclin dependent kinase inhibitor 2A (CDKN2A), allows tumor cells to bypass cell cycle checkpoints and enter G1 of the cell cycle (de Araújo *et al.*, 2016).

If caught at stage I or II, melanoma tumors are usually treated by surgical removal to prevent metastasis from occurring. Metastasis can occur during late stage melanoma and many therapies used to treat the melanoma are designed to target mutated proteins within mutated pathways. These small molecule inhibitors aim to cease the activity of the mutated proteins and halt the downstream effects of these signaling pathways. Some FDA approved drugs in this class used to treat melanoma are

vemurafenib, which inhibits mutated BRAF in the MAPK pathway and trametinib, which inhibits MEK1 and MEK2 to reduce MAPK activity (Cerchia *et al.,* 2017). γ-irradiation is a second type of therapy used during late stage melanoma treatment and involves using high-energy γ waves to directly damage the DNA of the tumors to kill them. However, many melanomas prove difficult to treat with these therapies as the tumors can evolve additional mutations to avoid the treatment. In the case of small molecule inhibitors, the tumor cells could develop a mutation allowing them to bypass the inhibitor, and in γ-irradiaiton, the tumors can gain resilience to the higher energy waves (Baskar *et al.*, 2012; Cerchia *et al.,* 2017).

Recently, immunotherapy has proven to be a promising form of melanoma treatment. Immunotherapy involves educating the patient's immune system to recognize and kill tumor cells. Ipilimumab, the first immunotherapy drug FDA approved to treat melanoma, is a cytotoxic T-lymphocyte-associated protein 4 (CTLA-4) antibody. CTLA-4 downregulates immune activity, therefore ipilimumab acts to reduce this function, allowing the immune system to better recognize and eliminate harmful tumors (Wolchok *et al.*, 2013). Although promising, immunotherapy still comes across the complication of tumors evolving new ways to avoid immune detection.

C. G Protein Coupled Receptors

G Protein-Coupled Receptors (GPCRs) are membrane bound receptors comprising the largest group of receptors in the human genome. All receptors in this family share the same basic structure: an extracellular ligand binding domain, a 7 transmembrane α helical domain, and an intracellular heterotrimeric G protein

containing the subunits Gα, Gβ, and Gγ. Upon ligand binding, the receptor undergoes a conformational change and the Gα is activated through an exchange of GDP for GTP via an enzyme called guanine nucleotide exchange factor (GEF). Once activated, Gα dissociates from Gβ and Gγ subunits to stimulate downstream effector protein(s), leading to the release of secondary messenger molecules to trigger a cellular response.

Receptor activity is highly dependent on the G protein coupled with it. There are multiple subgroups of Gα proteins such as Gαs, Gαi, or Gαq. The first two act on adenylate cyclase to stimulate or inhibit release of the secondary messenger cyclic AMP (cAMP). Meanwhile, the Gαq subunit interacts with phospholipase C (PLC) to generate the secondary messengers diacylglycerol (DAG) and inositol triphosphate (IP3). These secondary messengers interact with effector proteins to activate a variety of responses within the cell such as increasing cytosolic Ca^{2+} by opening calcium channels in the sarcoplasmic reticulum. Increased intracellular Ca^{2+} results in cell responses such as turning on/off transcription factors and the release of small molecules into the extracellular space, to name a few.

Currently GPCRs are classified into six categories depending on sequence homology. These categories are the rhodopsin-like receptors, the secretin receptors, the metabotropic glutamate receptors, the fungal mating pheromone receptors, the cyclic AMP receptors, and the frizzled/smoothened receptors. Receptors in each category are localized to different organ systems depending on their function. For example, glutamate, the ligand for metabotropic glutamate receptors, is a major neurotransmitter with excitability properties. Due to this, members of the

metabotropic glutamate receptors are mostly localized to the central nervous system where they function in memory and learning formation. Meanwhile, glucagon-like peptide receptors mediate glucagon signaling and are found on β cells of the pancreas. Finally the rhodopsin class GPCR receptor, known as the protease-activated receptor, is involved in thrombin signaling; their expression is high in platelets and can also be found in myocytes.

Given that GPCRs encompass the largest receptor group in the human genome, many drugs in development, and currently on the market, target GPCRs for therapy. Receptors in this vast group are linked to a wide variety of diseases across all organ systems. The aforementioned metabotropic glutamate receptors are linked to neurodegenerative disorders such as Huntington's disease and Alzheimer's disease (Mehta *et al.*, 2013). Meanwhile, prolonged activation of protease-activated receptors can lead to thrombosis (Leger *et al.*, 2006). These are only a few of the many diseases linked to GPCRs and their activity. In recent decades the discovery of the *mas* oncogene opens up the discussion for a potential link between these receptors and the transformation of normal cells into cancer cells (Young *et al.*, 1986). Proposing the possibility to target GPCRs as rational and novel therapeutic designs for the treatment of human cancers.

D. Metabotropic Glutamate Receptors

Glutamate is one of the 20 amino acids essential to building proteins and is found in many organ systems (Julio-Pieper *et al.*, 2011). This amino acid is the major neurotransmitter and its activity is linked to memory and learning formation. Due to

this crucial function, the organ system where glutamate's activity is well documented is the Central Nervous System (CNS) (Meldrum *et al.,* 2000) . There are two groups of receptors glutamate interacts with: the ionotropic glutamate receptors and the metabotropic glutamate receptors. Ionotropic glutamate receptors are ligand-gated ion channels that activate upon glutamate binding. When bound to ligand, iGluRs change to the open conformation, which allows an influx of cations into the neuronal cell in order to depolarize the cell. The normal function of iGluRs is neural plasticity, which is crucial for the brain to learn and form memories (Bliss *et al*., 1993).

The second group of glutamate receptors is the metabotropic glutamate receptors (mGluR). These membrane bound receptors belong to the GPCR family of receptors. Glutamate binding to mGluRs initiates a signaling cascade within the cell to mediate numerous activities through downstream effector molecules. There are three groups of mGluRs simply named Group I, Group II, and Group III. Group II and III mGluRs are coupled with inhibitory G protein, which reduces levels of the second messenger cAMP by inhibiting adenyl cyclase, and decreases signal transmission in the CNS and periphery nervous tissue (Schoepp *et al.,* 2001). Group I mGluRs are coupled with $G\alpha q$ protein and function to increase synaptic activity. When activated, the dissociated $G\alpha q$ activate Phospholipase C (PLC) and its downstream effector proteins leading to the eventual increase of Ca^{2+} in the cytosol (Lüscher *et al.,* 2010).

Metabotropic glutamate receptor 1 (mGluR1) is an essential mGluR, functioning in memory and learning formation (Menard *et al.,* 2012). The receptor contains four domains necessary for its function. The first domain is an extracellular N-terminus,

consisting of two lobes separated by an amino terminal domain (ATD) that gives the domain a “venus fly trap” like appearance. The ATD is where the ligand binds to initiate mGluR signaling. The second domain is located between the ATD and the transmembrane region of mGluR1 and is a cysteine rich domain (CRD) encompassing multiple cysteine residues bound by disulfide bonds and is crucial to the activation of mGluR1 after ligand binding. Following the CRD is the distinctive seven transmembrane domain (TMD), made up of alpha helices interconnected by intracellular loops. The final domain is the cytoplasmic tail domain (CTD) located after the transmembrane domain at the C-terminus of the receptor where it modulates G-protein coupling to the receptor (Niswender *et al* 2010).

Activation of mGluR1 occurs when its ligand, L-glutamate, binds to the “venus fly trap” extracellular ATD domain. Once ligand is bound, the receptor undergoes a conformational change and $G\alpha q$ dissociates from $G\beta/G\gamma$ complex to activate PLC. PLC hydrolyzes phosphatidylinositol (4,5)-bisphosphate (PIP2) into the second messenger molecules inositol 1,4,5-triphosphate (IP3) and Diacylglycerol (DAG) (Taylor *et al.*, 1991). IP3 and DAG stimulate the release of calcium from the endoplasmic reticulum (ER) into the cytosol. The released calcium can activate protein kinase C (PKC) leading to a phosphorylation cascade ending in the stimulation of pro-tumorigenic pathways such as the MAPK and PI3K/AKT pathways (Schonwasser *et al.*, 1998).

Since glutamate is the main neurotransmitter, it has been long understood that mGluRs are located in the CNS. As such studies on complications and disease involving mGluRs relate to CNS disorders. For example, mGluR over-activation is linked to

neurodegenerative diseases such as Parkinson's and Alzheimer's disease (Vernon *et al.*, 2007). In regards to cancers, Group I mGluR activity are postulated as possible mediators in the transformation of adult glial cells into gliomas (Zhang *et al.*, 2015). mGluR activity is linked to the proliferation and differentiation of neuro-progenitor cells into glial cells and stimulating the receptors with an mGLuR agonist has shown to increase MAPK activity in the neural cells (Zhao *et al.*, 2011).

Recent reports have established the notion that mGluRs are not restricted to neural tissue, but they are also expressed in periphery tissue such as skin, mammary, prostate, gastrointestinal (GI), and liver (Chang *et al.*, 2005; Pollock *et al.*, 2003; Wu *et al.*, 2012; Yu *et al.*, 2016). These receptors appear to act as oncogenes on these tissue types, implying a possible role mGluR signaling can have in transforming normal cells into tumor cells (Martino *et al.*, 2013).

E. Metabotropic Glutamate Receptor 1 in Melanoma

Hints of normal mGluR1 activity linked to cancer formation can be seen in the transformation of glial cells to the benign cancer known as glioma. Glial cells consist of three cell types that provide specialized functions such as oligodendrocytes providing insulation and support to neurons by wrapping myelin around the axon (Jakel *et al.,* 2017). When glial cells overexpresses Group I mGluRs, they undergo transformation into glioma cells. Experiments with neural progenitor cells reveal mGLuR5 expression in the early stages of embryo development (Jansson *et al.,* 2014). Stimulating these receptors with an mGluR5 agonist increases proliferation and differentiation of neural cells into glial cells through the MAPK pathway (Zhao *et al.,* 2011). After stem cell

differentiation, mGluR5 expression remains in the adult glial cells (Luyt *et al.*, 2004), indicating its potential significance in mediating proliferation of adult glial cells well after differentiation. Furthermore, when glioma cells are treated with L-quisqualic acid, an mGluR1 agonist, they undergo increased cell proliferation and survival (Zhang *et al.,* 2015). The activity of a Group I mGluR agonist resulting in these outcomes suggest mGluRs participate in the transformation of glial cells into gliomas. Most likely related to group I mGluR's function in the proliferation and differentiation of neural stem cells.

Although previously assumed localized in CNS tissue, mGluR1 was discovered to be expressed in peripheral tissue as well (Julio-Pieper *et al.,* 2011). Therefore it is important to consider the activities of these receptors in peripheral tissue cell types. Our lab previously demonstrated mGluR1 is expressed in about 60% of melanoma biopsies and 80% of melanoma cell line, but not in normal human melanocytes (Wangari-Talbot *et al.*, 2012b). Furthermore, aberrant mGluR1 expression in normal melanocytes correlates with cellular transformation *in vitro* and tumor development *in vivo* (Pollock *et al.,* 2003; Shin *et al.*, 2008). Expression and functionality of mGluR1 is required to maintain the transformed phenotype and tumorigenicity *in vitro* and *in vivo* (Martino *et al.,* 2013). Finally, glutamate has proven to be essential for the viability and growth of melanoma cells (Gelb *et al.*, 2015). These details about mGluR1 activity related to melanoma allow us to investigate the GPCR as a novel target for melanoma treatment.

Activated PI3K/AKT and MAPK pathways are associated with initiation of melanoma. Human melanoma cells confirmed to express mGluR1 (UACC903 and C8161)

demonstrate higher basal activity of these two pathways when compared to mGluR1-negative melanoma cell lines (C81-61, UACC930) and normal melanocytes (Wangari-Talbot *et al.,* 2012). Treating mGLuR1^{+} melanoma cells with an agonist increases the activity of these tumor pathways and in contrast, the addition of an antagonist decreases pathway activity. These data suggests that tumorigenic pathway signaling in mGluR1 expressing melanoma is dependent on receptor stimulation on the cancer cells (Namkoong *et al.*, 2007). Finally, when the receptor is bound to ligand, sustained stimulation of these pathways is maintained through a release of glutamate from the intracellular space to the extracellular space. Establishing an autocrine loop where the cell continually self activates its own mGluR1, and a paracrine loop to activate mGluR1 by neighboring cells (Burger *et al.*, 1999). Disrupting mGluR1 activity either by blocking the receptor or, at the least, inhibiting glutamate release will theoretically slow tumor growth.

F. Using Riluzole to Target Metabotropic Glutamate Receptor 1 for Therapy

The first lines of targeted drug treatment for late stage melanoma were small molecule inhibitors and an example of one of these drugs is vemurafenib. Vemurafenib reduces MAPK signaling by inhibiting mutated BRAF(V600E). However, despite promising early results in melanoma patients, many tumors develop resistance,to the inhibitor through mutations in downstream proteins, such as NRAS, and patients taking vemurafenib risk relapse (Nazarian *et al.*, 2010). Recently, immunotherapy has emerged as the treatment of choice. Immunotherapy is a drug therapy type used to educate a patient's immune cells to recognize and kill tumors. One of the first immunotherapy

drugs approved to treat melanoma is ipilimumab. This drug inhibits the immunosuppressing protein CTLA-4, allowing cytotoxic t lymphocytes to recognize and kill tumor cells (Lipson *et al.,* 2011). More recent therapies such as pembrolizumab and nivolumab antagonize programmed cell death protein 1 (PD1). PD1 is a surface protein that downregulates and suppresses T-cell activity, therefore these drugs encourage T-cell inflammatory response by antagonizing PD1 (Guo *et al.*, 2017). Although promising, this therapy has yet to prove to be effective among a broad spectrum of patients.

Considering the apparent significance of mGluR1 signaling in melanoma initiation and progression, the receptor is being investigated as a potential therapeutic target in treating the aggressive disease, potentially to be used in conjunction with either of the previously mentioned therapies. Silencing mGluR1 expression in melanoma cells with short interfering RNAs (siRNA), decreases tumorigenicity *in vivo* and reduces MAPK and PI3K/AKT leading to decreased proliferation and increased apoptosis respectively *in vitro* (Wangari-Talbot *et al.*, 2012). An *in vivo* mouse model containing an mGluR1 transgene demonstrates that inhibiting the transgene slows melanoma growth in the mouse (Ohtani *et al.*, 2008). These data demonstrate *in vitro* and *in vivo* the potential of targeting mGluR1 in melanoma therapy. Possibly to use in conjunction with immunotherapy to slow tumor growth while educating immune cells to recognize tumors.

Riluzole is FDA approved to treat Amyotrophic Lateral Sclerosis (ALS). ALS is a disease of the neuromuscular system where upper and lower motor neurons degenerate, leading to muscle weakness and eventual paralysis (Hardiman *et al.*, 2017).

Riluzole's exact mechanism of action is unknown, however one of its functions is to inhibit glutamate release from neural cells in order to slow excitation signals (Martin *et al.*, 1993). Taking into account the autocrine/paracrine effect seen in mGluR1 expressing melanoma cells, riluzole's glutamate release inhibitory action may allow it to functionally act as an inhibitor of mGluR1-mediated pro-cell-growth activity and thus can be explored as a potential candidate to treat mGluR1 expressing tumors including melanoma. Inhibiting glutamate release will reduce the autocrine/paracrine loops established by the tumor, thereby reducing the MAPK and PI3K/AKT pathway activity.

Previous *in vitro* studies on melanoma and breast cancer cells that express mGluR1 support that inhibiting the receptor's activity using an inhibitor slows cancer cell growth (Banda *et al.*, 2014; Le *et al.*, 2010). Riluzole's glutamate release inhibitory effect is thought to functionally inhibit receptor activity, supporting its potential use in treating mGluR1 expressing cancer types. A Phase 0 clinical trial of riluzole treatment in melanoma patients with resectable stage III/IV melanoma given the FDA-approved maximum dose of riluzole for 2 weeks demonstrated a significant decrease in phospho-AKT and phospho-ERK in 1/3 of the tumors resected, implying riluzole is negatively modulating the PI3K/AKT and MAPK pathways respectively (Yip *et al.*, 2009). A phase II trial of riluzole in patients with advanced melanoma showed decreased tumor volume in 1/3 of patients and 6 out of 13 patients who had rapid progression showed disease stabilization at first screening, 4 of which continued to have stable disease for 23-56 weeks (Mehnert *et al.*, 2018)

Although the biological evidence was present, disease stabilization was low across the patients; meaning riluzole at the maximum FDA approved dose by itself may not be sufficient in melanoma treatment. Riluzole has been shown to be a radiosensitizing agent in mGluR1^{+} melanoma cells, and it reduces tumor migration when mGluR1^{+} melanoma cells are exposed to it (Khan *et al.*, 2011; Le *et al.,* 2010). Finally, mGluR1 expressing melanoma cells exposed to riluzole demonstrate higher levels of cleaved PARP, suggesting that riluzole is inducing programmed cell death, or apoptosis, in these cell types (Wangari-Talbot *et al.,* 2012). These results support the notion that riluzole can be used in conjunction with other therapies to improve treatment efficacy.

In vitro exposure to riluzole reveal increased expression of the DNA damage marker γH2AX in mGluR1 expressing human melanoma cells. γH2AX denotes the phosphorylated histone H2AX, a phenomenon that occurs when a strand break is introduced in DNA. Moreover, cells treated with riluzole display lower levels of cytoplasmic glutathione levels and high cytosolic glutamate (Wall *et al.*, 2014). Glutathione is a Phase II metabolism enzyme that removes harmful free radicals from a cell that are the results of metabolic activities (Yin *et al.*, 2000). The observed decrease in glutathione and increase in glutamate points to the likelihood that riluzole disrupts the activity of the Glutamate-Cystine antiporter xCT. Cysteine is the rate limiting amino acid required in glutathione synthesis, however the amino acid is not synthesized within the cell. Instead, cells use xCT to export cytosolic glutamate in exchange for import of extracellular cystine (Figure 1). The cystine is reduced to form cysteine, which can be used to participate in glutathione synthesis. By disrupting the release of glutamate from

mGluR1 expressing melanoma cells, riluzole consequently disrupts the entry of cysteine into the cell, preventing glutathione synthesis. Without glutathione, reactive oxygen species will accumulate inside the cell and induce DNA damage (Wall *et al.,* 2014).

G. Oxidative DNA Damage and Repair

Chemical or physical insult to DNA can damage the integrity of chromosomal structure and DNA sequences. DNA damage is classified under one of two categories: endogenous DNA damage or exogenous DNA damage. Exogenous DNA damage is induced directly by an external source to the cell, such as a xenobiotic. Endogenous DNA damage is induced by compounds that result from the normal metabolic cellular activity, such as reactive oxygen species (Swenberg *et al.*, 2011). Common ways in which DNA damage can occur are through alkylation, radiation, or oxidation. Alkylating agents induce DNA damage through intra/inter cross-linking guanine bases, which prevents strands from uncoiling during replication or repair (Kondo *et al.*, 2010). Several types of radiation can damage DNA, UV radiation can form thymine dimers within adjacent thymine bases of a strand, while γ-radiation can directly induce strand breaks, and ionizing radiation attacks the deoxyriose backbone of the DNA molecule (Ward *et al.,* 1988). Lastly, oxidative damage occurs when ROS oxidizes nitrogenous bases in the DNA, most commonly guanine into 8-hydroxydeoxyguanosine, which can improperly pair with adenine, resulting in potentially harmful mutations (Barzilai *et al.,* 2004)

Our lab demonstrated that mGluR1 expressing melanoma cells exhibit DNA damage that correlates with an increase in ROS when treated with riluzole, suggesting

that riluzole induces endogenous oxidative damage. Moreover, cells treated with riluzole exhibit a decrease in glutathione, pointing to an inability for cells to remove ROS as a result of normal cell metabolism. Accumulating ROS can oxidize nitrogenous bases, most commonly guanine, and may lead to DNA damage in the form of inter/intra-strand cross links, mutation, or strand breaks.

An early step in the repair of DNA strand breaks is phosphorylation of Histone H2AX (γH2AX) and its presence in mGluR1 positive melanoma cells after riluzole treatment suggests DNA strand breaks occur during treatment (Wall *et al*., 2014). H2AX phosphorylation at Ser139 occurs rapidly after strand breaks and is commonly mediated by ataxia telangiectasia mutated (ATM). Once phosphorylated, the H2AX acts as an anchor for DNA repair complexes at the site of damage to maintain chromosome integrity and initiate repair (Kuo *et al.,* 2008). γH2AX is a common indicator of double-stranded DNA breaks (DSBs), however it is possible for single-stranded DNA breaks (SSBs) to persist into DSBs. In the case of SSBs, one protein to take into consideration is replication protein A (RPA).

RPA's normal function is to prevent single-stranded DNA (ssDNA) from winding back together after DNA helicase unwinds the strands. However, in the case of SSB induction, RPA acts in DNA damage recognition, excision, and repair in the nucleotide excision repair (NER) pathway. Like H2AX, RPA is also phosphorylated in response to DNA damage, particularly during genotoxic stressed introduced during mitosis (Anantha *et al.*, 2008). Phosphorylated RPA mediates DNA replication at the damage site; and in the case of SSBs, the unbroken strand can be used as a template to repair the strand

break. This objectively means that SSBs are more manageable to repair than DSBs since DSBs do not have a complimentarily stand readily available to guide the repair proteins.

Since DNA is essential in storing and passing the genetic information of organisms, a variety of mechanisms have evolved to repair any damage to maintain its integrity. Base excision repair (BER) and nucleotide excision repair (NER) are common mechanisms for repairing ssDNA. They involve identifying an abnormality within a strand of DNA, excising the abnormal base or nucleotide, and repairing with the appropriate base or nucleotide (Krokan *et al.,* 2013; Reardon *et al.,* 2005). For DNA double-stranded breaks, the major repair mechanisms are homologous recombination (HR) and non-homologous end joining (NHEJ).

These pathways are more complicated than BER and NER as they usually repair multiple bases and nucleotides. HR most commonly occurs in the G2/M and S phases of the cell cycle (Mao *et al.*, 2008). It requires a homologous sequence from a sister chromatid to guide repair proteins to add bases in the correct order. The use of the complimentary sequence allows HR to be an accurate repair pathway. Briefly, HR is initiated by Mre11-Rad50-Nbs1 (MRN) complex binding to the site of DNA damage. Rad51 binds to the 3'overhangs and forms a filament made of nucleic acids and protein to begin strand invasion. Once strand invasion is completed, DNA polymerase reconstructs a new strand using a complimentary sequence from a sister chromatid. Once this is completed, a cross shaped holliday junction is formed and is converted into recombination products by specialized endonucleases that only cut one strand of DNA (Jasin *et al.,* 2013).

NHEJ is a process present throughout the cell cycle that does not require a homologous sequence, and instead uses microhomologies present in single-stranded overhangs to guide repair (Mao *et al.,* 2008). This makes NHEJ less accurate than HR, but also makes it the common repair mechanism in G1 since it does not require the homologous sequence. In NHEJ a heterodimer consisting of Ku70/Ku80 that complexes with DNA-dependent protein kinases (DNA-PKs) to bridge the broken strands together. Nucleases remove nucleotides and bases that are later resynthesized by DNA polymerases. The ligation step is the final step in NHEJ and is mediated by the DNA ligase IV complex which can ligate strands across gaps (Lieber *et al.,*, 2010).

We hypothesize that riluzole interacts with xCT transporter, halting the efflux of glutamate and influx of cystine. The decrease in available cystine leads to a decrease in cysteine, resulting in depletion of the phase II enzyme glutathione. Consequentially resulting in an accumulation of reactive oxygen species resulting from normal metabolic processes that lead to endogenous DNA strand breaks.

In the presented study, we aim to indirectly and directly determine the type of DNA strand breaks induced by riluzole, whether it is SSBs or DSBs. We also explore which DNA repair pathway is utilized in riluzole induced DNA damage. Results from these investigations will provide the first steps toward the elucidation of riluzole's mode of action and provide knowledge on how to improve its therapeutic efficacy in mGLuR1 expressing tumor cells.

MATERIALS AND METHODS

A. Cell Culture

The cell line used throughout the following experiments is the established C8161 human melanoma cell line. C8161 is an mGluR1 expressing metastatic melanoma cell line derived from a patient, maintained in RPMI-1640 media (Sigma, St. Louis MO), 10% fetal bovine Serum (Sigma, St. Louis), and 1% of Pennicillin/Streptomycin (Sigma, St. Louis MO), referred to as R10. Once the cells reach about 80% confluence, the cells were split into their treatment groups for experimentation.

B. Antibodies

Anti-γH2AX antibody and anti-rabbit secondary were purchased from Millipore (Burlington, MA). Anti-phosphoRPA32 (Ser4/Ser8) was purchased from Bethyl Laboratories (Montgomery, TX). Anti-RPA32 was purchased from Santa Cruz Biotechnology (Dallas, TX). Anti-α-tubulin and anti-mouse IgG were purchased from Sigma (St. Louis, MO). Goat anti-mouse IgG (H+L) cross-adsorbed secondary antibody, alexa fluor 488 and goat anti-rabbit IgG (H+L) highly cross-adsorbed secondary antibody, alexa fluor 594 were purchased from Thermo Fisher Scientific (Waltham, MA).

C. Fixing Cells for Immunofluorescent Microscopy

Cells for immunofluorescent microscopy were grown to 80-90% confluence on coverslips in 35mm plates (Corning, Tewksbury, MA) for each treatment. The treatment groups were no treatment, vehicle (0.1% DMSO), 10mM N-Acetyl Cysteine (NAC), 10μM riluzole, 10μM riluzole + 10mM NAC, 20μM riluzole, and 20μM riluzole + 10mM NAC for 24, 48, and 72 hours. To allow time to attach, cells in each plate were treated at 24

hours post-passage. At their respective time points, cells were washed with 1X phosphate buffered saline (PBS) and fixed with 3% paraformaldehyde for 10 minutes at room temperature. Fixed cells were kept at 4^0C until Immunostaining.

D. Immunostaining

Cells were washed with 1X PBS four times and incubated with 0.5% Triton X-100 solution for 5 minutes at 4^0 C. After incubation, cells were exposed to anti-pRPA and anti-RPA32 or anti-γH2AX primary antibody using dilutions as recommended by each vendor for 20 minutes at 37^0 C. After incubation with the primary antibody, the cells were washed three times with 1X PBS and incubated with alexa fluor-488 and alexa fluor-594 conjugated secondary antibody for 20 minutes at 37^0 C to image green fluorescent protein and red fluorescent protein respectively on a single coverslip. Cells were washed four times with 1X PBS and stained with DAPI to visualize cell nuclei. The coverslips were sealed onto microscope slides using nail polish and examined under a confocal fluorescent microscope.

E. Whole Cell Protein Lysate Extraction

About $3x10^5$ cells were plated onto each 60mm tissue culture plate (Corning, Tewksbury, MA) designated for treatments. The treatment groups were no treatment, vehicle (0.1% DMSO), 10mM NAC, 20µM riluzole, and 20µM riluzole + 10mM NAC for 24 and 48 hours. Before treatment cells were starved in serum free RPMI media for 48 hours to synchronize the cells. At each specified time point, the media was aspirated and cells were washed twice with 1X PBS. Extraction buffer was prepared in a 3:1 volumetric water:laemmli sample buffer (Bio Rad, Hercules, CA) ratio plus β-

mercaptoethanol (Sigma, St Louis, MO). Depending on the cell confluence at the time of collection, 80-120µL of extraction buffer was added to each plate and cells were scraped into a 1.5mL eppendorf tube and incubated at 99^0 C for 10 minutes in a glycerol hotplate bath. The mixtures were centrifuged in a Z 36 HK refrigerated high-speed centrifuge (Labnet, Edison, NJ) at 14,0000 RPM for 10 minutes at 4^0 C and the supernatants were collected and kept at -80^0 C.

F. Western Blot Analysis

Equal volume of protein lysate was loaded into each well of 10% SDS gel after denaturation at 95°C for five minutes. A reference protein ladder (Precision Plus Protein Standards-Bio-Rad, Hercules, CA) was used to determine the size of the band. Gels were electrophoresed for 1 hour at room temperature at 150 volts. Next, the proteins were transferred onto a nitrocellulose membrane (GVS North America) at 160mA for 2 hours at 4°C. Once transferred the membranes were stained with Ponceau S Red (Sigma, St Louis, MO) to visualize the transferred proteins. The membranes were then cut according to target protein size and blocked in 5% nonfat dry milk solution containing Tris buffered saline + Tween 20 (TBST) for 1 hour. After blocking, the membranes were incubated in anti-γH2AX primary antibody at 1:500 or anti-pRPA primary antibody at 1:1,000 overnight at 4°C on a rocking platform. For anti-α-tubulin, the membranes were incubated in antibody diluted to 1:10,000 for 20 minutes at room temperature on a rocking platform. The next day, membranes were washed with TBST using a SnapID (Millipore, Burlington, MA) 5 times and incubated in anti-rabbit secondary antibody or anti-mouse IgG secondary antibody diluted to 1:5,000 for 1 hour at room temperature

on a rocking platform. After incubation with the secondary antibody, the membranes were washed 5 times in TBST with the SnapID, exposed to ECL HRP substrate (Millipore, Burlington, MA), and bands were imaged using GeneSys imaging software.

G. Cell Harvesting and Lysis in Agarose

About $3x10^5$ C8161 cells were plated onto 60mm tissue culture plates. The cells were starved in serum free RPMI media for 48 hours for synchronization. The treatments were: no treatment, vehicle (0.1% DMSO), 10mM NAC, 20µM riluzole, and 10mM NAC + 20µM riluzole. At 48 hours after treatment the cells were trypsinized and centrifuged at 1,000RPM for 10 minutes. After centrifugation the media was aspirated and the cells were resuspended in 1X PBS at a concentration of $1.0x10^6$ cells/mL, 2,000 cells were pipetted into 1% low melting agarose on a comet assay slide containing a thin layer of agarose (Trevigen, Gaithersburg, MD) and incubated at 4°C for 30 minutes. After incubation the cells were lysed in lysis buffer (Trevigen, Gaithersburg, MD) over night at 4°C.

H. Neutral Conditioned COMET Assay

The COMET assay slides were removed from the lysis buffer and excess buffer was drained off the slides. Slides were immersed in 50mL of 1X neutral electrophoresis buffer (Tris Base, Sodium Acetate, adjust to pH=9 with glacial acetic acid 10X diluted to 1X with ddH_2O) for 30 minutes at 4°C. Approximately 850mL of 1X neutral electrophoresis buffer was added to the CometAssay® ES unit (Trevigen, Gaithersburg, MD) and the slides were immersed in 1X neutral buffer in the slide tray, covered with a slide tray overlay, and electrophoresed at 21 volts for 45 minutes at 4°C. After

electrophoresis, excess buffer was drained from the slides and slides were immersed in DNA precipitation solution (7.5M Ammonium Acetate, ddH_2O) for 30 minutes at room temperature. Afterwards, the slides were fixed in 70% ethanol for 30 minutes at room temperature. In order to bring all the cells to a single plane for observation, the samples were dried on a heat block at 37°C for 15 minutes.

I. Alkaline Conditioned COMET Assay

The COMET assay slides were removed from the lysis buffer and excess buffer was drained off the slides. The slides were immersed in 50mL of alkaline unwinding solution (200mM EDTA pH 8, NaOH pellets, ddH_2O) for 1 hour at 4°C in the dark to unwind the DNA. Approximately 850mL of 1X alkaline electrophoresis buffer (500mM EDTA pH 8, NaOH pellets, ddH_2O) was added to the CometAssay® ES unit and the slides were immersed in 1X alkaline buffer in the slide tray, covered with a slide tray overlay, and electrophoresed at 21 volts for 30 minutes at 4°C. After electrophoresis, excess buffer was drained from the slides and immersed twice in deionized water for 5 minutes to remove residual buffer and then fixed in 70% ethanol for another 5 minutes, all at room temperature. To bring the cells to a single plane for observation, the samples were dried at 37°C for 15 minutes on a heat block.

J. Propidium Iodide Staining

Slides processed under both COMET assay conditions were stained with 50µL of 2µg/mL propidium iodide (PI) diluted to 1:100. The samples were incubated at room temperature for 30 minutes protected from light. After incubation the slides were washed in water for 5 minutes to remove any background PI. The slides were then dried

on a heat block set to 37^{o}C and examined under a confocal fluorescent microscope at 10X magnification.

K. DNA Repair Inhibitor Treatment

C8161 Cells were plated into 12 well plates at 2.0x10^{5} cells/well. The cells were treated with either the Rad51 inhibitor B0$_2$ (Millipore, Burlington MA) or the DNA PK inhibitor Nu7026 (Millipore, Burlington MA) at a concentration of 10µM for 6 hours. After pretreatment with the DNA repair inhibitors the cells were treated with either 10µM etoposide, vehicle (0.1% DMSO), or 20µM riluzole for 24 and 48 hours. At the end of the treatment the cells were processed for flow cytometry

L. Fixing Cells for Flow Cytometry

At 24 or 48 hours post-treatment the cells were trypsinized and centrifuged at 1,000 RPM. The media was aspirated and the cell pellet resuspended in 1xPBS. The cells were washed twice in PBS by centrifuging the cells for 10 minutes at 1,000 RPM. Cells were fixed in 1mL of 70% ice-cold methanol added drop wise while vortexing to ensure all cells are fixed evenly. The cells were then incubated in methanol for 20 minutes at -20^{0}C. After fixation, cells were washed twice and resuspended in 1% Bovine Serum Albumin in PBS and stored at 4^{0}C until staining.

M. Immunostaining for Flow Cytometry

100µL of 0.5% Ipegal (Sigma, St Louis MO) was added to fixed C8161 cells and incubated for 15 minutes in the dark at room temperature to permeabilize the cells. After permeabilization, the cells were washed with 2mL of 0.1% Ipegal by centrifuging the samples at 1,500 RPM for 7 minutes, aspirating the supernatant, and resuspending

the pellet in the remaining volume (approximately 50-100 μL). Next, the cells were blocked with 500μL normal rabbit serum (Thermo Fisher, Waltham MA) diluted at 1:20 for 15 minutes at room temperature. After blocking, the C8161 cells were washed with PBS and incubated with anti-γH2AX antibody diluted at 1:300 for 60 minutes at room temperature. After primary antibody incubations, the cells were washed in PBS and incubated in Alexa fluor-488 conjugated antibody diluted to 1:400 for 60 minutes at room temperature protected from light. After incubation with the secondary antibody the cells were brought to flow analysis and analyzed for intercellular γH2AX.

N. Statistical Analysis:

All statistical analysis was performed using StatPlus statistical software (AnalystSoft, Walnut, CA). Statistical significance between mean values of treatment groups was determined using a one-way ANOVA with bonferronis correction. Data are presented as a mean +/- standard error of mean (SEM), pith a $p<0.05$ considered statistically significant.

RESULTS

A. Phosphorylated histone H2AX localization to the nuclei of C8161 is mediated by reactive oxygen species:

Histone H2AX is phosphorylated (γH2AX) immediately after induction of DNA double-stranded breaks (DSBs). The function of γH2AX is to localize to the sites of the breaks within the chromosome and recruit DNA repair proteins to initiate repair of the breaks (Kuo *et al.,* 2008)). We used immunofluorescent (IF) microscopy to visualize the presence of γH2AX after exposing mGluR1-expressing melanoma cells to riluzole at various time points. Our lab previously demonstrated the induction of the phosphorylated histone after riluzole treatment in mGluR1 expressing melanoma cells using this approach. One of the known functions of riluzole is to inhibit the export of glutamate to the extracellular environment (Martin *et al.,* 1993). Here we sought to establish our initial findings and evaluate any possible effect N-Acetyl Cysteine (NAC) may have on the induction and localization of this DNA damage marker. NAC serves to alleviate DNA damage induced by reactive oxygen species (ROS) through the donation of a cysteine to the cell. This will allow the cells to synthesize glutathione even if riluzole were to inhibit the cystine/glutamate antiporter (xCT) from importing cystine that can be reduced to cysteine, the rate-limiting component of glutathione. Therefore glutathione, an important antioxidant, can remove ROS that result from metabolic processes, and prevent damage to DNA and γH2AX induction even when riluzole is present.

For this set of experiments we used the chemotherapeutic etoposide as the positive control due to its capability of inducing DNA strand breaks. Etoposide's mechanism of action is to inhibit topoisomerase II activity, preventing the re-ligation of DNA strands, and resulting in DNA strand breaks (Burden *et al.,* 1998). C8161 human melanoma cells were plated out one day prior to treatment. The treatment groups are: no treatment, vehicle (0.1% DMSO) with or without NAC, 10μM etoposide, and 10μM or 20μM riluzole with or without NAC. Etoposide treatment was only for 30 min, the optimal time for the induction of DNA strand-breaks determined previously in our lab. Vehicle, riluzole treatments, and no treatments were for 24, 48 and 72 hours with or without NAC. We detected a clear induction of γH2AX foci localized to the nuclei of etoposide treated C8161 cells (Figure 2). C8161 cells under conditions of no treatment, treated with vehicle (0.1% DMSO) or 10mM NAC showed very little γH2AX foci (Figure 3, left panel). Under similar conditions C8161 cells treated with 10μM or 20μM riluzole for 24 hours exhibit dense γH2AX foci localized to the nuclei of the cells (Figure 3, right panel) compared to no treatment, vehicle or NAC treated cells (Figure 3). Furthermore, when NAC is present in the media with either concentration of riluzole tested, a reduction in dense γH2AX foci localized to the nuclei is observed (Figure 3, right panel). These data imply that γH2AX induction by riluzole is reduced when NAC is present in the medium.

A similar trend can be seen at the 48 and 72 hour time points, where we observe dense γH2AX foci localized to the nuclei of cells that were treated with only riluzole (Figures 4 and 5). At the 48 hour time point a greater induction of γH2AX foci in the

nuclei compared to C8161 cells treated with 10μM or 20μM riluzole for 24 hours (Figures 3, 4, and 5). The amount of foci and intensity at the nuclei after 72 hour treatment appears to be similar to the 48 hour treatment, though these samples had higher cell density, possibly due to the longer time of treatment (Figure 5). At both 48 hour and 72 hour time points, γH2AX foci is denser and greater in the riluzole treated C8161 cells than in the no treatment and vehicle (0.1% DMSO) treated cells (Figures 4 and 5). When NAC is included alongside riluzole we observed a decrease in foci formation in the 48 hour treatment to levels similar as the foci induction observed in the vehicle (0.1% DMSO) treated cells (Figure 4). However this decrease does not appear as substantial in the 72 hour treatment, possibly due to persistent damage over time by riluzole's action during this time point (Figure 5).

B. Replication protein A is phosphorylated after riluzole treatment in the cytoplasm of mitotic cells:

Replication protein A (RPA) is a protein whose normal function is to prevent single-stranded DNA from winding back together after being unwound by DNA helicase. In the incidence of mitotic DNA stress, RPA binds to single-stranded DNA and is phosphorylated to initiate DNA repair (Anantha *et al.,* 2008). As a result, phosphorylated RPA (pRPA) can be used as an indicator of potential single-stranded DNA breaks (SSBs), induced by riluzole. Similar to the set of experiments for γH2AX, we used a 30 minute 10μM etoposide treatment as our positive control for single-strand break induction (Figure 6). The inhibition of topoisomerase II leading to DNA strand breaks during mitosis can result in pRPA induction (Liu *et al*., 2012). C18161 cells were

plated at 24 hours prior to treatments and the treatment groups for this experiment were no treatment, vehicle (0.1% DMSO), and 10μM or 20μM riluzole with or without NAC for 24, 48, and 72 hours.

After treating C8161 melanoma cells with riluzole for 24 hours, a slight induction of pRPA can be observed by an increase in the cytoplasm of the cell, indicated by green fluorescence (Figure 7, right panel). Compared to the riluzole treatment groups, cytosolic phosphorylated RPA is not induced to a similar extent in no treatment or vehicle (0.1% DMSO) treated cells (Figure 7, left panel). Although we observed pRPA in the cytosol, across all treatment groups the total RPA32 (stained red) is localized to the nuclei of the cells (Figure 7). At the 24 hour time point, the riluzole with NAC group demonstrate reduced levels of cytosolic pRPA similar to those seen in the vehicle (0.1% DMSO) group (Figure 7), suggesting the presence of NAC led to a decrease in pRPA and presumably much less single-stranded DNA breaks.

At the 48 and 72 hour time points, we observed hyper-phosphorylated RPA in the cytoplasm of cells treated with riluzole only (Figures 8 and 9, right panels). The DAPI staining of these riluzole treated cells revealed condensed nuclei localized to the center of cells displaying hyper-phosphorylated RPA, potentially indicating that these cells are in the mitotic phase of the cell cycle (Figure 10). RPA is phosphorylated in response to DNA damage induced during mitosis and these effects induced by riluzole were not seen when NAC is included in the treatment, hinting at the notion that NAC is mitigating phosphorylation of the SSB marker, pRPA (Figures 8 and 9, right panels). These results

reinforce the notion that DNA strand breaks induced by riluzole is likely due to ROS accumulation potentially brought about from reduced glutathione synthesis.

C. Protein markers for double-stranded DNA breaks and single-stranded DNA breaks are elevated after riluzole treatment:

After visualizing the DNA damage markers using IF microscopy, we used Western blots to quantify the expression of these proteins after riluzole treatment. For this set of experiments, the cells were serum starved for 48 hours to synchronize the cells, allowing the C8161 cells to have a uniformed response to riluzole treatment. Cells were plated into treatment groups 24 hours prior to starvation to ensure cell adhesion to the tissue culture plates. The experimental groups were no treatment, vehicle (0.1% DMSO) and 20μM riluzole with or without NAC. Our positive control for both protein markers was a 0.5 hr 10μM etoposide treatment (Figures 11 and 12, panel A). Whole cell protein lysate was collected to examine the protein levels of γH2AX and pRPA at 24 and 48 hours post treatment.

Parallel to what we observed in IF microscopy, Western blot band intensities demonstrate elevated levels of both γH2AX and pRPA in C8161 cells treated with riluzole compared to vehicle control cells at both 24 and 48 hour time points (Figures 11 and 12, panel A). We used NIH Image J software to quantify band intensities and normalized to corresponding vehicle (0.1% DMSO) treatments (Figures 11 and 12, panel B). We demonstrated that at 24 hours, riluzole treated cells exhibit a 2-fold increase in both γH2AX and pRPA compared to vehicle (0.1% DMSO) was detected (Figure 11, panel B). A one-way ANOVA statistical test reports a statistically significant increase in γH2AX but

not pRPA when normalized to vehicle treatment (0.1% DMSO) (Figure 11, panel B). Further evaluation with a compare means T test shows a significant increase in γH2AX expression in riluzole only treated cells compared to vehicle (0.1% DMSO) treatment (Figure 11, panel B). When NAC is present in the media along with riluzole, we observed a reduction in DNA damage protein marker levels similar to that observed in the vehicle (0.1% DMSO) treated cells (Figure 11, panel B).

Quantification of bands from the 48 hour treatments demonstrates a comparable trend; however, instead of a 2-fold increase relative to vehicle (0.1% DMSO) treatment we detected a 1.5-fold increase in expression of both proteins in the riluzole treatment group (Figure 12, panel B). A one-way ANOVA demonstrates no statistical significance in the γH2AX or pRPA Western Blots. Interestingly, γH2AX induction is marginally higher than pRPA induction at this time point (Figure 12, panel B). However unlike in the 24 hour treatments, this trend demonstrates no statistical significance. When C8161 cells are treated with 20μM riluzole and NAC, a reduction in both γH2AX and pRPA expression to levels almost seen in vehicle treatment was detected (Figure 12, panel B).

D. Riluzole induces DNA damage under both neutral and alkaline conditioned COMET assays.

Immunofluorescent microscopy and Western immunoblots experiments are indirect measurements of DNA strand breaks; in order to take a more direct look at DNA strand breaks we implored the COMET (single-cell gel electrophoresis) assay. This assay permits one to differentiate between single-stranded breaks (SSBs) and double

stranded-breaks (DSBs) by performing the COMET assay under two conditions: alkaline and neutral. The alkaline condition contains a DNA unwinding, step, which allows SSBs and DSBs to migrate out of the nucleus under an electric field, making it nonspecific to the type of DNA damage detected. Meanwhile the neutral condition does not contain a DNA unwinding step, meaning only DSBs can migrate out of the nucleus, allowing the assay to be specific for DSBs. Under both conditions, negatively charged damaged DNA will migrate out of the nuclei during the electrophoresis step, forming the "tail" of the comet. Meanwhile, undamaged DNA remains within the nuclei, forming the comet "head", the longer the tail length, the more DNA damage a cell endured.

For this set of experiment we first plated out $3.0x10^5$ cells/60mm cultured plate and 24 hours later we removed the serum for 48 hours to synchronize the cells. After synchronization the cells were subjected to the following treatments: no treatment, vehicle (0.1% DMSO), and 20µM riluzole with or without NAC for 48 hours. At the end of treatment period, the cells were removed, washed with twice PBS and 2,000 cells were embedded in 1% agarose on each agarose-coated slide. The cells were then electrophoresed in a neutral or alkaline buffer for 45minutes at 21volts.

The control we used for the COMET assay is bleomycin, an antibiotic with unique anti-tumor activity. This compound is known to induce both types of DNA strand breaks via the formation of free oxygen radicals (Dorr *et al.,* 1992). Bleomycin's oxidative mechanism of action allows it to act as an optimal positive control for our COMET assay experiments. As expected, clear tail formation was seen in bleomycin treated C8161

cells under the alkaline condition and the neutral condition COMET assays (Figures 13 and 14, panel A).

Under both neutral and alkaline conditions the formation of comet tails was evident in riluzole treated C8161 cells (Figures 13 and 14, panel A). Tails form when broken DNA migrates from the nuclei of lysed cells during electrophoresis. Qualitatively, it is difficult to determine if tails in the riluzole treatment group appear longer than tails in the no treatment and vehicle (0.1% DMSO) groups, especially in the alkaline COMET assay condition (Figures 13 and 14, panel A). Under the neutral condition the addition of NAC in the growth media appears to reduce the tail length induced by riluzole (Figure 14, panel A). Qualitatively, this decrease is not distinguishable when the COMET assays were performed under the alkaline condition (Figure 13, panel A).

E. Comparison of neutral condition and alkaline condition COMET assays suggest oxidative DNA damage induces double-stranded DNA breaks over single-stranded DNA breaks

Using the Nikon instruments elements analysis software (Nikon, Melville NY) we can measure the tail moments of individual cells. The tail moment is measured as the sum of half the radius of the comet head and half the length of the come tail. This measurement is a more accurate representation of DNA damage because it takes into consideration the damaged and undamaged DNA. We used Graphpad Prism 6 software to plot tail moments of individual cells onto scatter column plots to emphasize tail moments in individual cells within a treatment group and then compared them to the

group average of that treatment (Figures 13 and 14, panel B). Although there is a degree of variability across treatment groups electrophoresed under both neutral and alkaline conditions, most cells contain tail moments similar to the mean length of their respective treatment groups (Figures 13 and 14, panel B). When comparing the tail moments between treatment groups, riluzole treatment increases tail moment compared to no treatment or vehicle (0.1% DMSO) treated samples (Figures 13 and 14, panel B). Under both the alkaline and the neutral conditions, the increased tail moment induced by riluzole is reduced when NAC is present in the growth media (Figures 13 and 14, panel B). This decrease is much greater in the neutral conditioned cells than in the alkaline conditioned cells (Figures 13 and 14, panel B). These results are comparable to the ones observed in the Western blots where riluzole treatments induced elevated levels of DNA damage associated protein.

Quantifying and comparing tail moments between both comet assay conditions displays the trend we observed in our IF and western blots (Figure 15). C8161 cells treated only with riluzole revealed higher levels of DNA damage indicated by statistically significant tail moment increases when compared to vehicle (0.1% DMSO) control treatment (Figure 15). Under both conditions we observed about a 1.5 fold increase in tail moments compared to vehicle (0.1% DMSO) treated cells (Figure 15). However, when NAC is included in the growth media with riluzole, there is a difference between neutral and alkaline conditions. In the alkaline condition we still see a statistically significant increase in tail moment when NAC is present in the media of riluzole treated cells compared to cells treated with only riluzole (Figure 15). In contrast, the tail

moment formed under the neutral condition demonstrated a reduction to levels below significance and similar to the vehicle treated cells (Figure 15), suggesting that inclusion of NAC rescues cells from riluzole induced oxidative damage. These COMET assay results showed that riluzole treatment most likely induce DNA double-strand breaks rather than single-stranded breaks.

F. Riluzole Induced DNA Damage is Increased when Non-Homologous End Joining Repair Pathway is Inhibited

In order to observe the effect of DNA DSB repair pathways on riluzole induced DNA DSBs we used intercellular flow cytometric analysis of γH2AX levels after riluzole treatment with or without an inhibitor of the DNA repair pathways, non-homologous end-joining (NHEJ) and homologous recombination (HR). The assay requires the use of fluorescent-tagged antibodies to detect γH2AX induction through flow cytometry as read-outs of DNA damage. For this experiment, we synchronized C8161 cells in 100mm tissue culture plates for 48 hours. After synchronizing the cells, we plated $2.0x10^5$ cells into each well of a 12 well plate. At 24 hours later the cells were given treatments: vehicle (0.1% DMSO) and 20μM riluzole with or without DNA repair inhibitor for 24 or 48 hours.

The NHEJ inhibitor we used is Nu7026, which is a small molecule inhibitor of DNA-dependent protein kinase (DNA-PK). Briefly, Nu7026 is a competitive inhibitor of DNA-PK, which prevents Ku70 binding to strand breaks and recruiting DNA-dependent protein kinase catalytic subunit (DNA-PKcs) to facilitate rejoining the broken DNA strands (Veuger *et al.*, 2003). The inhibitor we used to block HR activity is the specific

Rad51 inhibitor known as B02. This inhibitor prevents Rad51 from polymerizing onto single-stranded overhangs of DSBs, preventing reciprocal and nonreciprocal DNA strand exchange by homologous duplexes (Alagpulinsa *et al.*, 2014). By inhibiting DSB repair pathways with these inhibitors, we expect to differentiate which repair pathway is utilized in riluzole-treated cells.

To confirm that the assay was a viable approach in measuring increases in DNA damage induction using γH2AX levels as read-outs when either repair pathway is inhibited, we treated C8161 cells with etoposide as a control. Cells were pretreated with either Nu7026 or B02 for 6 hours and treated with 10μM etoposide for 24 hours. After treatment, the cells were stained with a fluorescent-tagged γH2AX antibody followed by flow cytometry. Our assay demonstrated an increase in γH2AX expression in cells pretreated with either inhibitor compared to cells treated with no inhibitor (Figure 16).

In C8161 cells, at 24 hours, we detected an increase in cell populations within the fluorescent gate across all riluzole treated groups compared to DMSO (Figure 17), indicating the induction of DNA strand-breaks is increased in riluzole treatments. We compared the percent of cells gated with fluorescence between vehicle (0.1%DMSO) and riluzole treatments, and it is apparent that elevated γH2AX levels were detected in riluzole treated ones (Figure 17). In C8161 cells pretreated with the competitive DNA-PK inhibitor Nu7026, a statistically significant increase in γH2AX levels was seen compared to vehicle (0.1% DMSO) with Nu7026 and riluzole without inhibitor treatments (Figure17). C8161 cells when pretreated with the specific Rad51 inhibitor B02, γH2AX

levels were similar to levels seen in riluzole treated cells without any inhibitors (Figure 17). C8161 cells treated with riluzole for 48 hours showed very little change in γH2AX levels across all treatment groups relative to DMSO (Figure 18). These results were very similar to the Western blots where γH2AX expression levels induced by riluzole were the highest at 24 hours and decreased at 4 8hours (Figure 18). Taken together these findings point to a possible role of NHEJ in repairing riluzole induced DNA DSBs in C8161 cells.

Discussion

Our lab showed that aberrant expression of a normal neuronal receptor, metabotropic glutamate receptor 1 (mGluR1) in melanocytes is sufficient to transform normal melanocytes *in vitro* and induce spontaneous malignant melanoma *in vivo (Pollock* et al., *2003)*. The elevated glutamate levels in mGluR1 expressing cells ensure the constitutive activation of the receptor through an autocrine/paracrine loop maintains the activities of two major signaling cascades, mitogen-activated protein kinase (MAPK) and the phosphatidylinositol 3-kinase protein kinase (PI3K/AKT) pathways, which create a sustainable cell proliferative environment for the tumor cells (Pollock *et al*., 2003; Shin *et al*., 2008). Further investigation of mGluR1 receptor activity in melanoma cells shows that antagonizing mGluR1 function or expression level results in decreased cell growth *in vitro* and tumor progression *in vivo* plus an increase in apoptosis (Namkoong *et al.,* 2007; Wangari-Talbot *et al.,* 2012).

Among the various anti-mGluR1 compounds tested, riluzole showed promising results. Riluzole is FDA approved to treat ALS due to one of its functions, the ability to inhibit glutamate release from the intracellular space to the extracellular environment (Martin *et al.,* 1993). This allows riluzole to act as a functional inhibitor by disrupting the autocrine/paracrine loops in mGluR1 expressing cells. In preclinical studies using several human melanoma cell lines, we demonstrated the induction of apoptotic cell death in *in vitro* and *in vivo* (Namkoong *et al.,* 2007). Based on these preclinical results we performed a pilot study (phase 0 trial) in patients with resectable stage III/IV melanoma. We administered the maximum FDA-approved dose of riluzole to patients

for 2 weeks prior to their definitive resection. We found that 4/12 patients had significant decreases in FDG-PET scans, decreased levels of pERK and pAKT in the post- vs pre-treatment tumors, and significant tumor shrinkage (Yip *et al.,* 2009). We then conducted a therapeutic phase II trial of single-agent riluzole in patients with advanced melanoma, whose primary endpoint was response rate by RECIST criteria (Mehnert *et al.,* 2018). A significant reduction in tumor volume was noted in 1/3 of the patients, but all initial responses were mixed. However, 6 out of 13 patients who initially had rapidly progressive disease were found to have stable disease at first screening and 4 patients continued with stable disease for 23-56 weeks (Mehnert *et al.,* 2018). These results support mGluR1 as a novel therapeutic target for the treatment of late stage melanoma.

We reported earlier that riluzole has the potential to induce DNA damage in mGluR1 expressing melanoma cells (Wall *et al.,* 2014). For this study, we sought to perform more detailed examinations and to identify the specific type of DNA damage mediated by riluzole in mGluR1 expressing human melanoma cells. First we aimed to discriminate the type of DNA strand breaks induced by riluzole by differentiating double-stranded DNA breaks (DSBs) or single-stranded DNA breaks (SSBs). Distinguishing between these two DNA damage responses is significant because DSBs are harder for cells to repair than SSBs due to a lack of a complimentary sequence for repair proteins as read-outs making them more toxic to the cell. DNA damage has dramatic consequences. Acute effects stem from disturbance of DNA metabolism, such as transcription and replication, triggering transient or permanent cell cycle arrest or cell

death. Long-term effects arise from irreversible mutations, lead to loss or alteration of gene function.

We used immunofluorescent (IF) microscopy to visualize the induction and location of DNA damage protein markers and western blots to examine their expression in mGluR1 expressing human melanoma cells after riluzole treatment. We hypothesize that riluzole induced DNA damage by ROS is due to loss or a reduction in glutamate/cystine exchange function of xCT. A decrease in the influx of cystine will prevent cells from synthesizing the phase II enzyme, glutathione, to remove ROS. This is because the rate-limiting step in glutathione synthesis is the reduction of cystine, an amino acid that is not readily available in the cell, to cysteine (Meister *et al.,* 1995). Hence, for these experiments we included a treatment group where cells are treated with N-acetylcysteine (NAC) along with riluzole. NAC acts to prevent ROS-induced DNA damage by donating a cysteine to the cells, allowing them to synthesize glutathione and eliminate ROS as a result of metabolic processes (van Zandwijk *et al.,* 1995). NAC will help to provide evidence of whether or not riluzole may be inhibiting xCT in mGluR1 expressing melanoma cells. In the presence of NAC, C8161 cells will synthesize glutathione even if riluzole inhibits glutamate release by blocking xCT activity. This will reduce the induction of DNA strand breaks and their protein markers by riluzole compared to riluzole only treatment.

We examined phosphorylated Histone H2AX (γH2AX) as a marker for DSBs and phosphorylated Replication Protein A (pRPA) as a marker for SSBs. γH2AX is a well-known indicator of double-strand breaks in DNA as the phosphorylated histone

functions to localize to the site of the DSB and initiate repair proteins shortly after DSBs are introduced within the chromosome (Kuo *et al.,* 2008). RPA is well-known to bind to single-stranded DNA during replication, however it can bind to single-stranded DNA during mitotic DNA stress where it is phosphorylated at Ser4/Ser8 to initiate repair (Anantha *et al.,* 2008). Meaning the phosphorylated form of RPA can be used as an indicator of SSBs.

Our IF results confirmed that an increase in the DSB protein marker, γH2AX, occurs in mGluR1 expressing melanoma cells after riluzole treatment compared to vehicle (0.1% DMSO) and untreated controls. When examining γH2AX levels, we detected an increase in the number of dense foci localized to the nuclei of cells in 10μM and 20μM riluzole treatment groups across 24, 48, and 72 hour time points. This phenomenon is reduced when NAC is included in the riluzole treated cells. The number and intensity of γH2AX foci in the nuclei of cells decreases across the three time points. Western blot analysis of γH2AX reflects what we observed in IF microscopy, we detected increased γH2AX band intensities in riluzole treated samples that is decreased when NAC is included in the media. When normalized to vehicle treated samples the increased γH2AX expression is the highest at the 24 hour time point and is reduced during the 48 hour treatment. This is likely due to phosphorylation of Histone H2AX being an early event after DSB induction. At both 24 and 48 hour time points with the addition of NAC the γH2AX expression levels were reduced almost to vehicle treatment levels. These results support the notion that riluzole induced DSBs is most likely due to an accumulation of ROS through the depletion of glutathione resulting from decreased

xCT activity and with the addition of NAC, cystine is supplied and participated in glutathione synthesis. These western immunoblot results confirmed our IF observations.

Moreover, when evaluating pRPA in IF microscopy, we observed an increase in pRPA staining in the cytoplasm of cells treated with 10μM and 20μM riluzole and the phenomenon is evident across 24, 48 and 72 hour treatments. The phosphorylated RPA levels appeared to be higher at the 48 and 72 hour time points compared to the 24 hour ones. Examining the DAPI stains of riluzole treated samples at 48 and 72 hour reveal condensed nuclei localized to the center of the cells, suggesting that these cells may be at the mitotic phase. Riluzole has been shown to induce G2/M cell cycle arrest (Namkoong *et al.,* 2007), suggesting the pRPA induction may be due to mitotic stress induced by riluzole activity. Similar to the results in γH2AX, pRPA induction by riluzole is also related to ROS formation as these outcomes are diminished when NAC is added with riluzole at both concentrations tested. Riluzole induced DNA damage in the form of SSBs may occur as genotoxic stress during mitosis. The subsequent western blot experiments reflect similar observations as in IF microscopy. The riluzole mediated induction of pRPA was detected in the cytosol of cells, therefore we elected to collect whole cell protein lysate as opposed to nuclear protein lysate only to ensure we collected all pRPA induced by riluzole. The western blots showed a clear induction of pRPA by riluzole in the form of increased protein band intensities. A reduction in the protein band intensities was noted with the addition of NAC, and articulates that pRPA expression induced by riluzole is dependent on ROS accumulation. Quantifying pRPA reveals a clear increase in this SSB marker after 24 hour riluzole treatment. Similar to

γH2AX, the increase in pRPA expression is higher in 24 hour and lower at the 48 hour time point, but overall when normalized to the same amount of total protein; riluzole mediated induction of SSBs specified by pRPA levels are less than the induction of DSBs designated by γH2AX expression level in westerns. This could point to a possibility that DSBs induction by riluzole activity is more severe than SSBs induction. Our results also point to that SSBs induced by riluzole is most likely caused by ROS because these effects are reduced when riluzole is treated along with NAC. NAC rescue of this DNA damage protein further supports the concept that riluzole may be inhibit the glutamate/cystine antiporter xCT.

Western blots and IF microscopy only illustrate what is happening at the protein level, meaning these assays are indirect methods to measure DNA damage response to riluzole. In order to have a more direct look at DNA damage we utilized the COMET assay. Cells used for this assay are embedded in agarose and can be electrophoresed under two conditions, alkaline and neutral. The cells in the alkaline condition have a DNA unwinding step prior to electrophoresis, which allows the assay to detect DSBs and SSBs, making it nonspecific. The neutral condition does not contain this step, allowing the assay to be specific for detecting DSBs. Earlier when we initially examined the genotoxicity of riluzole in mGluR1 expressing melanoma cells, we only performed the alkaline conditioned assay (Wall *et al.*, 2014). Therefore, it was nonspecific and served only to demonstrate DNA damage induced by riluzole. In order to further distinguish the type of DNA damage induced by riluzole, we performed the COMET assays under

both conditions. This allows us to distinguish whether strand breaks as a result of oxidative stress induced by riluzole is single-stranded or double-stranded.

Similar to the IF and western blot results; we observed increased damage upon riluzole treatment in COMET assays under both conditions. However, with the addition of NAC there is clearly a reduction in tail moments only in neutral conditioned COMET assays to levels similar as the vehicle treated groups. Addition of NAC did not modulate the tail moments at all in alkaline conditioned COMET assays. These results showed that the majority of riluzole-induced DNA damage is likely to be DSBs and not SSBs. Qualitatively our results showed DNA damage across the no treatment group as well. This may be due to factors related to the cell passage or the handling of cells during processing, particularly prior to lysis where the cells were pipetted up and down with a micropipette to mix the cells. This could sheer the cells, and lead to the displayed DNA damage we observed in this treatment group.

Taken together, IF microscopy, western immunoblots and COMET assays all pointed to the presence of DNA double-stranded breaks in riluzole treated samples. Upon the induction of DSBs, the DNA damage response plays a crucial role in maintaining genomic integrity. This prevents the development of cancer through cell cycle checkpoint arrest and ensures that the DNA repair occurs prior to the resumption of the cell cycle. Cells have evolved two main pathways to repair DSBs, non-homologous-end joining (NHEJ) and homologous recombination (HR).

NHEJ is the DSB repair pathway present throughout the cell cycle in mammalian cells and requires no homologous sequence for repair proteins to read off (Mao *et al.,*

2008). A crucial protein in NHEJ repair is DNA-dependent protein kinase (DNA-PK) which complexes with Ku70/Ku80 to initiate repair of DSBs through this pathway (Veuger *et al.,* 2003). We pretreated C8161 cells with a small molecule competitive inhibitor of DNA-PK, Nu7026; to examine riluzole induced DNA damage when NHEJ is inhibited. HR is another DNA DSB repair pathway and unlike NHEJ, is a pathway that utilizes the base sequence from a sister chromatid to polymerize new DNA strands; and because of this HR is a pathway most used in G2/M of the cell cycle once the DNA has been synthesized in S phase (Mao *et al* 2008). Rad51 plays a pivotal role in the recognition of the strand breaks and intrastrand cross links initiate repair, and as such we used the specific Rad51 inhibitor B02 to inhibit HR repair pathway in C8161 cells prior to riluzole treatment.

We used flow cytometric intracellular staining to examine the induction of γH2AX via a fluorescent-tagged antibody by riluzole while one or the other repair pathway is repressed. Pretreatment with the NHEJ inhibitor, Nu7026 followed by 24 hours with riluzole, we detected a three-fold increase in γH2AX induction compared to the vehicle (0.1% DMSO) control. Meanwhile using the same conditions as the NHEJ inhibitor but using the HR inhibitor, B02, we observed a 1.5 fold-change in γH2AX levels compared to vehicle (0.1% DMSO) treated cells, which is similar as riluzole treated cells in the absence of either inhibitor. The higher induction of γH2AX during NHEJ inhibition suggests the importance of this repair pathway in riluzole induced DNA damage. When we analyzed cells at 48 hour post-riluzole only, riluzole plus Nu7026 pretreatment or riluzole plus BO2 pretreatments, γH2AX induction was very comparable as the vehicle (0.1% DMSO) treatment group. These results mirror our western immunoblot results

where the phosphorylated histone was decreased from 24 to 48 hour riluzole treatments. This is likely due to γH2AX induction being an early phenomenon when chromosomes endure DSBs. Over time it is possible for the histone to be dephosphorylated as cells undergo DSB repair or apoptosis.

We utilized IF and western immunoblot techniques to indirectly observe the induction of SSBs and DSBs in mGluR1 expressing human melanoma cells after riluzole treatment. With both different but complementary approaches we showed the induction of protein markers, γH2AX for DSBs and pRPA for SSBs, increased after riluzole treatment relative to vehicle (0.1% DMSO) treatment. We then used the COMET assays to directly measure the induction of DNA DSBs and SSBs by electrophoresing riluzole treated cells under the neutral and alkaline conditions respectively and demonstrated the induction of both strand breaks by riluzole. For both the indirect and direct approaches when we included the cysteine donator, NAC, in the growth media, NAC mitigates the induction of both DNA damage evident by the reduction of respective protein markers and a decrease in DNA damage is seen under the neutral COMET assay but not under the alkaline COMET assay. Taken together, these data support the notion that DNA damage induced by riluzole is through endogenous oxidative stress leading to DNA DSBs.

These results ascertain that functionally inhibiting mGluR1 function with riluzole induces DNA DSBs rather than SSBs that may be easier to repair in melanoma cells. To further elucidate the mechanism of how riluzole induces this DNA damage through oxidative stress we will investigate the impact of riluzole on the glutamate/cystine

antiporter, xCT. We have on hand mouse melanocytes derived from a C3H/HeSnJ muse with spontaneous deletion in the last exon encoding xCT (Slc7a11) resulted in no detectable xCT protein (Chintala *et al.*, 2005). We will introduce exogenous xCT into these cells and compare the responses to riluzole. .

An interesting find we present in this study is a possible role of NHEJ in repairing riluzole induced DNA DSBs. By pre treating C8161 cells with a DNA-PK inhibitor and halting NHEJ in these cells we see a 3-fold increase in γH2AX 24 hours after riluzole treatment compared to vehicle (0.1% DMSO) treated cells. Further research can be conducted to establish the importance of NHEJ in repairing riluzole induced DNA DSBs over HR. We will want to see if we observe similar effects *in vivo*. Our results demonstrate increased DSBs induced by riluzole when NHEJ is inhibited *in vitro*, but *in* vivo combination studies will reveal what happens in a whole organism. NHEJ is a repair mechanism not exclusive to cancer cells, as many healthy normal cells use NHEJ to repair DNA. Therefore *in vivo* studies will provide information on not only efficacy, but of potential secondary toxic effects when combining riluzole with an NHEJ inhibitor for melanoma treatment.

There are limitations to the presented study, first and most obvious of which is that we conducted our experiments on one cell line. In order to build a stronger case for riluzole induced DSBs as a result from ROS we will run these experiments on another cell line. One such cell line we can use is the UACC903 cells line, like C8161 this is a human melanoma cell line that expresses mGluR1. Another limitation to the study is our results come solely from *in vitro* experiments. The nature of such experiments

means cells are exposed to much higher amounts of drug than they would realistically in a whole organism, whether *in vivo* or in patient. Western blot analysis can be done on *in vivo* protein lystate collected from tumors or treated animals to look for the DSB and SSB protein markers. It is also possible to run the COMET assay on such experiments, however it is a more difficult procedure than its *in vitro* counterpart because of an additional cell isolation step needed prior to embedding the cells in agarose.

Future directions of this project is to first directly measure riluzole's potential effect on the normal function of xCT. The reduction in tail moment as well as in DNA protein damage markers in riluzole treated cells with NAC compared to riluzole alone indirectly suggests riluzole activity results in xCT inhibition. Melanoma cells have shown to be highly dependent on glutathione to mitigate oxidative stress. Additionally a study on p53 mediated tumor suppression reveals p53 activity inhibits xCT function and results in ferroptosis, or iron dependent cell death (Jiang *et al.*, 2015). Hallmarks of ferroptosis include the accumulation of lipid peroxidases and glutathione depletion (Bertrand *et al.,* 2017). The results in the present study indicate it may be worthwhile to examine the potential effects of riluzole on p53 induction in these cells as an increase in p53 activity induced by riluzole would theoretically inhibit xCT depleting glutathione and accumulating lipid peroxidases resulting in DSBs due to oxidative stress. In addition, it may even be possible for riluzole itself to act on xCT similar to p53, resulting in ferroptosis and DNA DSBs as a result of ROS from lipid peroxidases.

As more research is conducted on mGluR1 and its relation to cancer, the more apparent its role in initiation and progression of tumor types becomes. Our lab has

done extensive research of mGluR1 and how it relates to melanoma development and as such we are looking into it as a therapeutic target for the debilitating disease. However others have shown mGluR1's role in tumor progression in other cancer types, such as triple negative breast cancer (TNBC). TNBC is a highly aggressive form of breast cancer with very little effective treatments available to patients. It has been demonstrated that TNBC cells can express mGluR1 and that antagonizing receptor activity on these cells can slow tumor growth (Speyer *et al*., 2012). Additionally, inhibiting the receptor has also recently shown to slow tumor growth and angiogenesis in non-small cell lung cancer (Hui *et al*., 2016). Other cancer types that express mGluR1 include hepatocellular carcinoma and prostate cancer (Wu *et al.,* 2012, Ali *et al*., 2014). The results from the present study points to a direction in understanding if targeting mGluR1 in these cancer types with riluzole leads to DNA double stranded breaks as it does in melanoma cells expressing mGluR1. Opening up the discussion in targeting the receptor as a therapeutic option in these cancer types as well.

G-protein coupled receptors (GPCRs) make up a significant portion of the human genome. Coupled with their activity being linked to the development of many different disorders, many drugs on the market and in development target this receptor family to achieve their therapy. The role of GPCRs in cancer development has only begun to be described within the recent decades because of the discovery of the *mas* oncogene (Young *et al.,* 1986). Since then, the role of GPCRs in cancer has been demonstrated in a variety of different types of the disease, suggesting these receptors can be a target in cancer therapy. Unlike small molecule inhibitors, GPCR inhibitors do not need to enter a

cell to exert their action because their targets are on the cell membrane. Compared to γ-radiation, drugs that inhibit GPCRS will target cells that express the receptor target and not healthy cells that do not. For example, mGluR1 is not normally expressed in healthy melanocytes; therefore riluzole cannot inhibit the activity of these normal cells. Finally, compared to immunotherapy, these drugs will act directly on the cancer itself and not rely on the ability of immune cells to recognize and kill tumor cell.

The human relevance of mGluR1 expression in various cancer types has been supported to an extent *in* vitro, *in vivo*, and clinically. Targeting this receptor may prove a more efficient therapy across these different cancer types. Establishing the mechanism by which riluzole induces DNA DSBs in melanoma cells will bring up the discussion of whether or not the functional mGluR1 inhibitor can induce DSBs in these other cancer types as well. This could potentially lead to the development of "broad spectrum" therapies that can be used in conjunction with other therapies, such as immunotherapeutic drugs, to slow tumor growth and improve the lives of millions of patients across the globe.

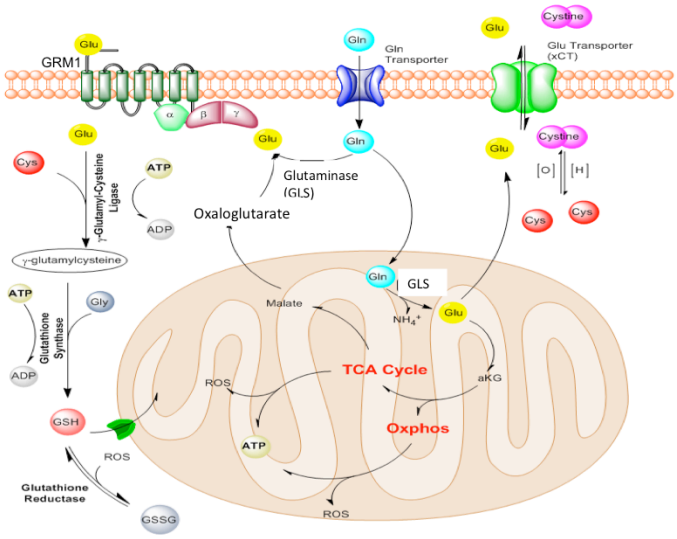

Figure 1. A graphic displaying the known roles of glutamate inside the cell.

The above diagram illustrates the various activities of glutamate inside of the cell. We hypothesize that riluzole inhibits the glutamate/cystine antiporter xCT from transporting glutamate out of the cell and cystine into the cell. This would lower the amount of available cystine to be reduced into cysteine for glutathione synthesis. Reducing glutathione levels while simultaneously increasing glutamate levels inside the cell. The inhibition of this transporter will also reduce the autocrine/paracrine effect of continuously stimulating mGluR1 on the cell surface.

Modified from Wall *et al.*, 2014.

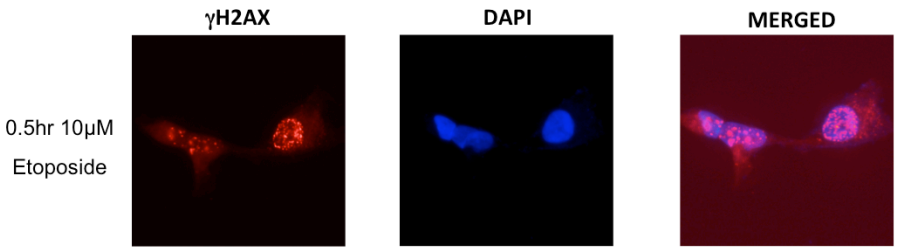

Figure 2. Immunofluorescent microscopy of γH2AX (red) and DAPI stain (blue) in C8161 cells treated with etoposide for 0.5-hours. Cells were plated onto cover slips in 35mm tissue culture plates. Etoposide (10μM) was given 24hours later. The cells were fixed in 3% paraformaldehyde at 0.5hour time point and stained for γH2AX (red) and DAPI stains for nuclei (blue). Images were taken at 10X magnification using a confocal fluorescent microscope.

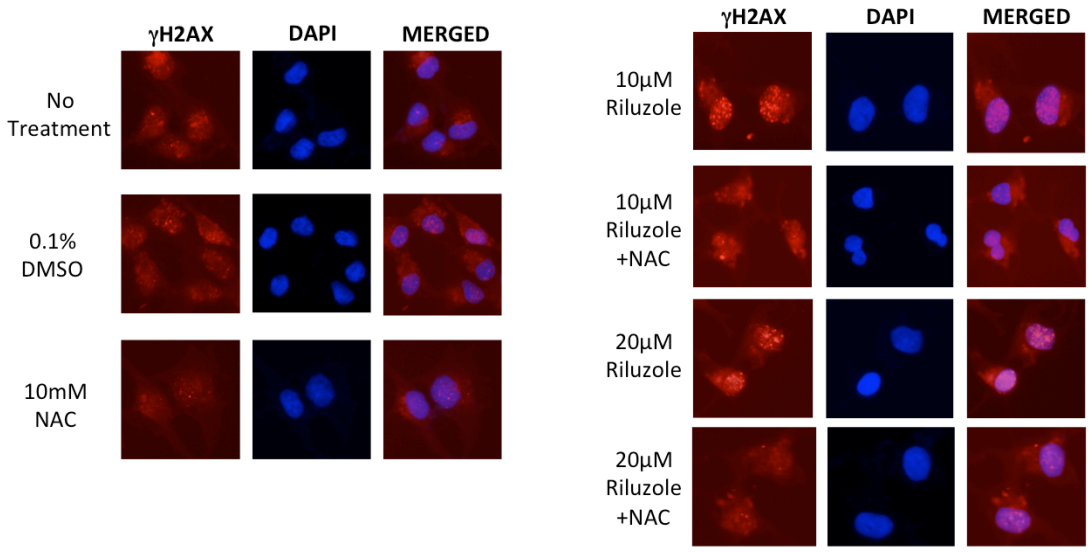

Figure 3. Immunofluorescent microscopy of γH2AX (red) and DAPI stain (blue) in C8161 cells treated with riluzole for 24-hours. Cells were plated onto cover slips in 35mm tissue culture plates. Vehicle (0.1% DMSO) or riluzole(10 or 20μM) was given 24hours later with or without NAC (10mM). The cells were fixed in 3% paraformaldehyde at 24hour time point and stained for γH2AX (red) and DAPI stains for nuclei (blue). Images were taken at 10X magnification using a confocal fluorescent microscope.

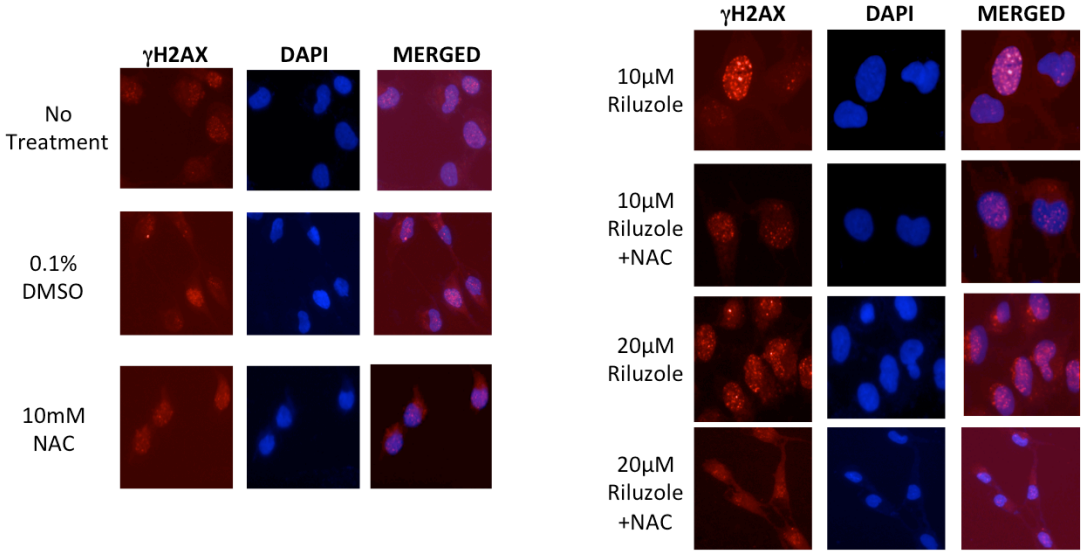

Figure 4. Immunofluorescent microscopy of γH2AX (red) and DAPI stain (blue) in C8161 cells treated with riluzole for 48-hours. Cells were plated onto cover slips in 35mm tissue culture plates. Vehicle (0.1% DMSO) or riluzole(10 or 20μM) was given 24hours later with or without NAC (10mM). The cells were fixed in 3% paraformaldehyde at 48hour time point and stained for γH2AX (red) and DAPI stains for nuclei (blue). Images were taken at 10X magnification using a confocal fluorescent microscope.

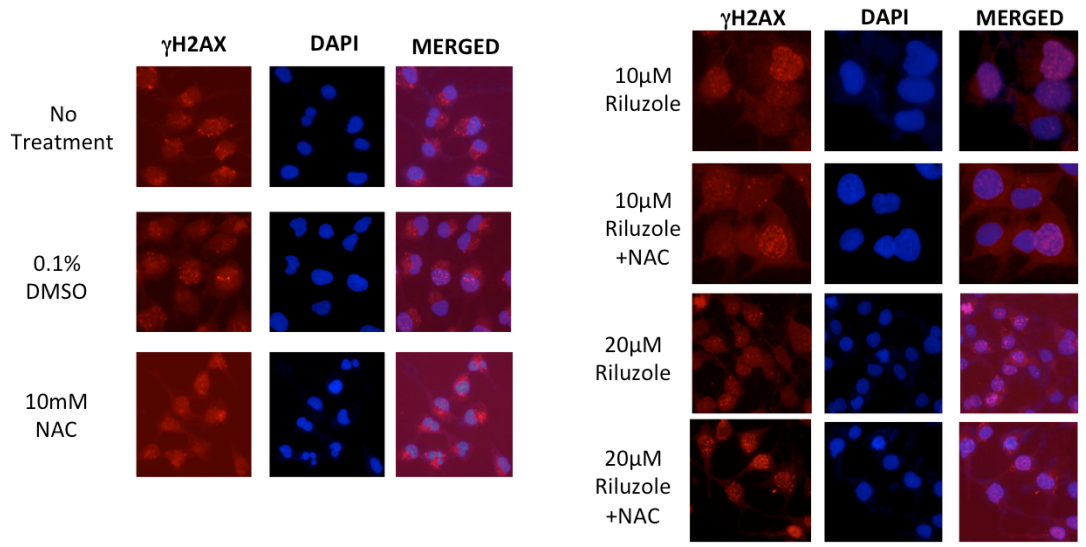

Figure 5. Immunofluorescent microscopy of γH2AX (red) and DAPI stain (blue) in C8161 cells treated with riluzole for 72-hours. Cells were plated onto cover slips in 35mm tissue culture plates. Vehicle (0.1% DMSO) or riluzole(10 or 20μM) was given 24hours later with or without NAC (10mM). The cells were fixed in 3% paraformaldehyde at 72hour time point and stained for γH2AX (red) and DAPI stains for nuclei (blue). Images were taken at 10X magnification using a confocal fluorescent microscope.

55

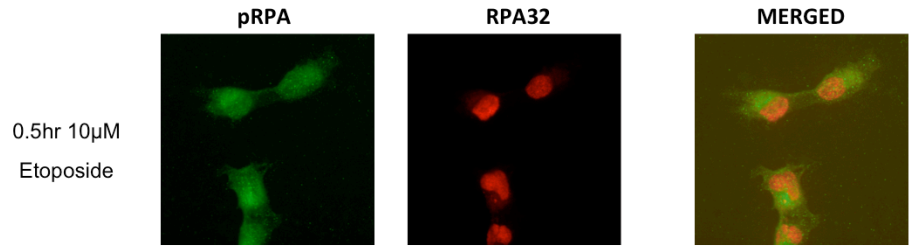

Figure 6. Immunofluorescent microscopy of phosphoRPA (pRPA) (green) and RPA32 (red) in C8161 cells treated with etoposide for 0.5-hours. Cells were plated onto cover slips in 35mm tissue culture plates. Etoposide (10μM) was given 24hours later. The cells were fixed in 3% paraformaldehyde at 0.5hours time point and stained for pRPA (green) and RPA32 (red). Images were taken at 10X magnification using a confocal fluorescent microscope.

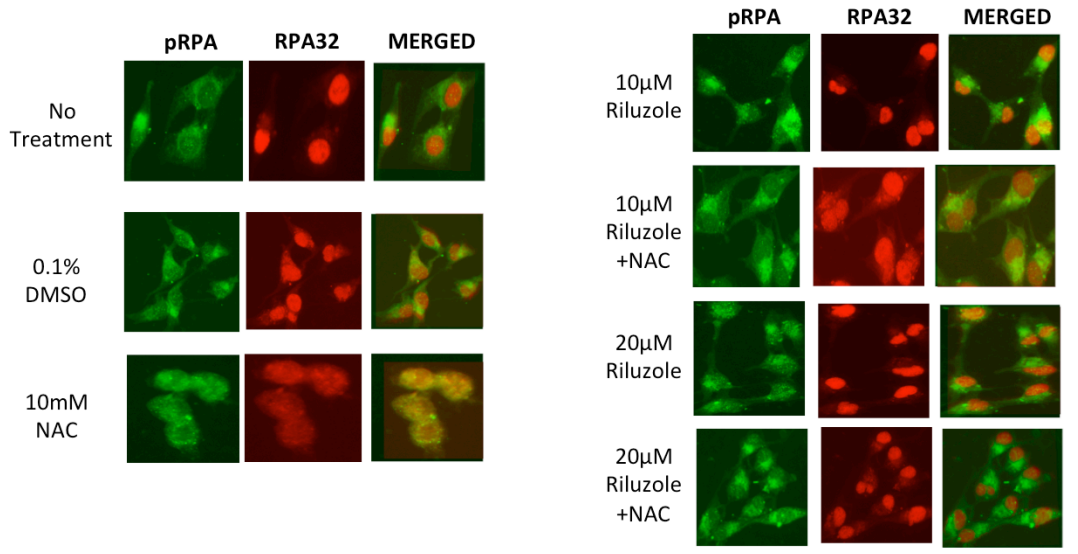

Figure 7. Immunofluorescent microscopy of phosphoRPA (pRPA) (green) and RPA32 (red) in C8161 cells treated with riluzole for 24-hours. Cells were plated onto cover slips in 35mm tissue culture plates. Vehicle (0.1% DMSO) or riluzole(10 or 20µM) was given 24hours later with or without NAC (10mM). The cells were fixed in 3% paraformaldehyde at 24hour time point and stained for pRPA (green) and RPA32 (red). Images were taken at 10X magnification using a confocal fluorescent microscope.

57

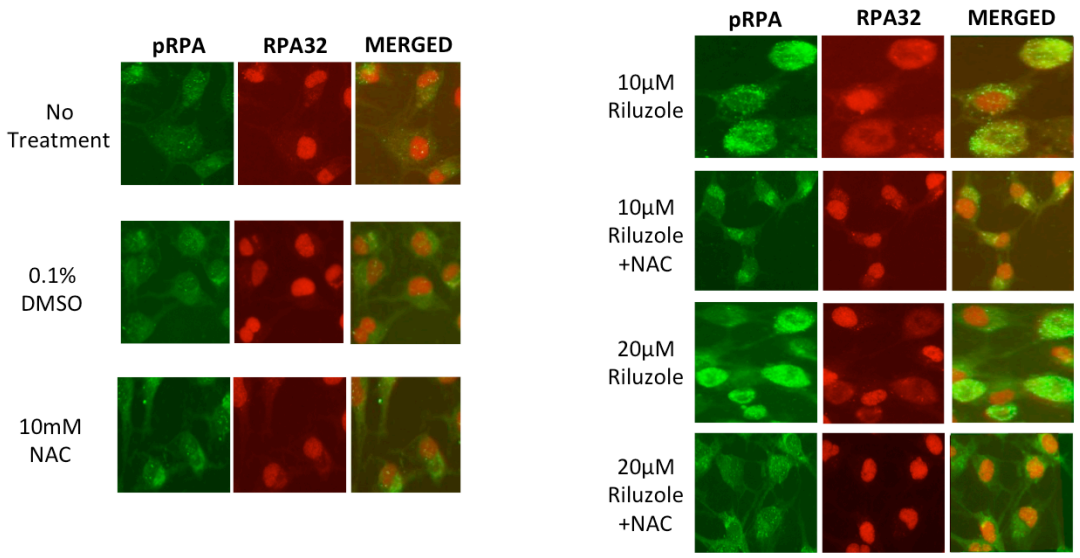

Figure 8. Immunofluorescent microscopy of phosphoRPA (pRPA) (green) and RPA32 (red) in C8161 cells treated with riluzole for 48-hours. Cells were plated onto cover slips in 35mm tissue culture plates. Vehicle (0.1% DMSO) or riluzole(10 or 20µM) was given 24hours later with or without NAC (10mM). The cells were fixed in 3% paraformaldehyde at 48hour time point and stained for pRPA (green) and RPA32 (red). Images were taken at 10X magnification using a confocal fluorescent microscope.

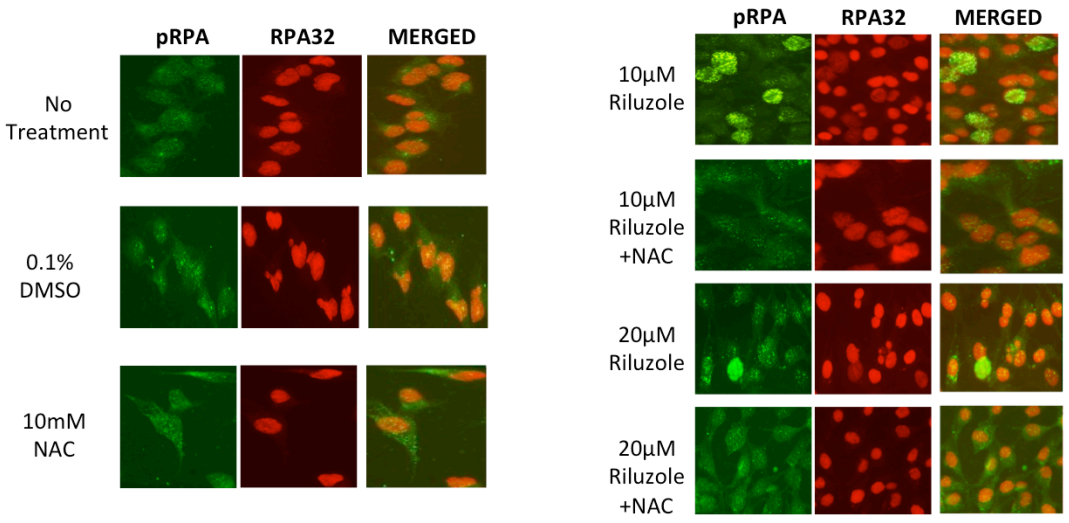

Figure 9. Immunofluorescent microscopy of phosphoRPA (pRPA) (green) and RPA32 (red) in C8161 cells treated with riluzole for 72-hours. Cells were plated onto cover slips in 35mm tissue culture plates. Vehicle (0.1% DMSO) or riluzole(10 or 20µM) was given 24hours later with or without NAC (10mM). The cells were fixed in 3% paraformaldehyde at 72hour time point and stained for pRPA (green) and RPA32 (red). Images were taken at 10X magnification using a confocal fluorescent microscope.

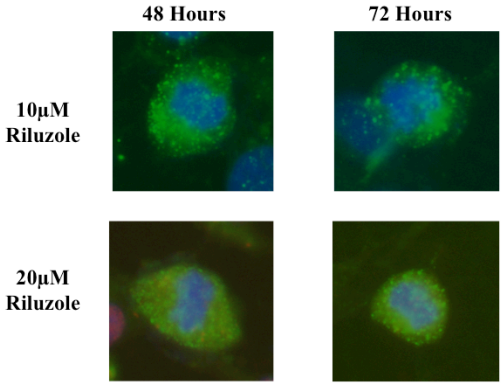

Figure 10. Immunofluorescent microscopy of phosphoRPA (pRPA) (green) and DAPI stains (blue) in C8161 cells treated with riluzole for 48 and 72-hours. Cells were plated onto cover slips in 35mm tissue culture plates. Riluzole(10 or 20µM) was given 24hours later. The cells were fixed in 3% paraformaldehyde at 48 and 72hour time points and stained for pRPA (green) and DAPI stains for nuclei (blue). Images were taken at 10X magnification using a confocal fluorescent microscope.

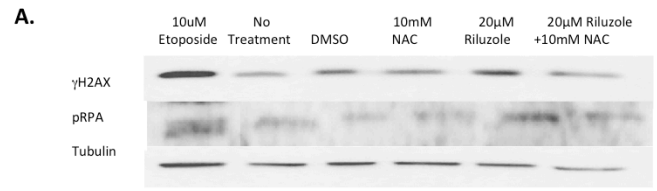

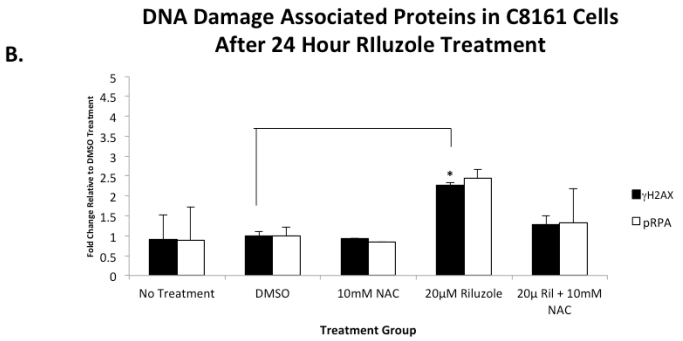

Figure 11. DNA damage protein expression after 24-hour riluzole treatment western blot bands (A). Quantifications of bands (B).
C8161 cells were analyzed for relative protein expressions of DNA strand break markers γH2AX and pRPA. Cells were serum starved for 48hours in 60mm tissue culture plates. Vehicle (0.1% DMSO) or riluzole(20µM) was given 24hours later with or without NAC (10mM). Whole cell protein lysate was collected at the 24hour time point. Data were normalized to tubulin protein expression and presented as mean relative protein expression to DMSO +/-SEM (n=3). An unstacked one-way ANOVA analysis found a $p<0.05$ for γH2AX and $p=0.17491$ for pRPA. An asterisk (*) indicates statistical significance in a compare means T test compared to vehicle group.

61

A.

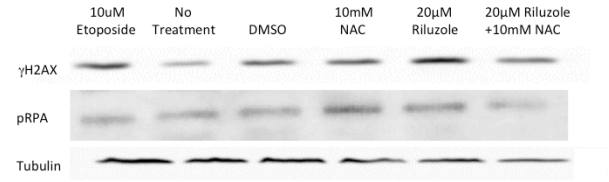

B.

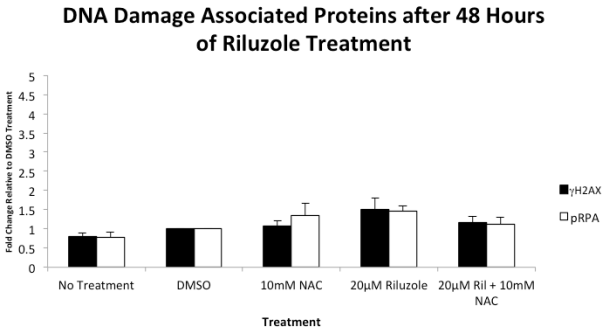

Figure 12. DNA damage protein expression after 48-hour riluzole treatment western blot bands (A). Quantification of band intensity (B).
C8161 cells were analyzed for relative protein expressions of DNA strand break markers γH2AX and pRPA. Cells were serum starved for 48hours in 60mm tissue culture plates. Vehicle (0.1% DMSO) or riluzole(20µM) was given 24hours later with or without NAC (10mM). Whole cell protein lysate was collected at the 48hour time point. Data were normalized to tubulin protein expression and presented as mean relative protein expression to DMSO +/-SEM (n=5). An unstacked one-way ANOVA analysis found a p value of 0.07261 for γH2AX and 0.09821 for pRPA.

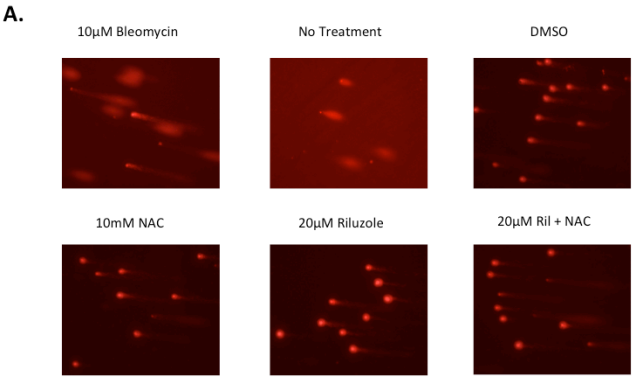

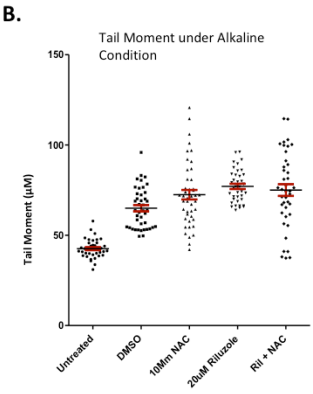

Figure 13. Alkaline condition comet assay images after 48-hour riluzole treatment (A) and tail moment comparison across treatments (B). Double- and single-stranded DNA breaks induced by riluzole was observed using the alkaline COMET assay. Cells were serum starved for 48hours in 60mm tissue culture plates. Vehicle (0.1% DMSO) or riluzole(20µM) was given 24hours later with or without NAC (10mM) and cells were embedded in 1% agarose on a COMET slide at 48hour time point. DNA was stained using propidium iodide diluted to 1:100. Images were taken at 10X magnification using a confocal fluorescent microscope (A). Individual tail moments were calculated by measuring the radii and the tail length of individual cells and adding half the radius to half the tail lengths. Graph was generated using Graphpad Prism 6 (B).

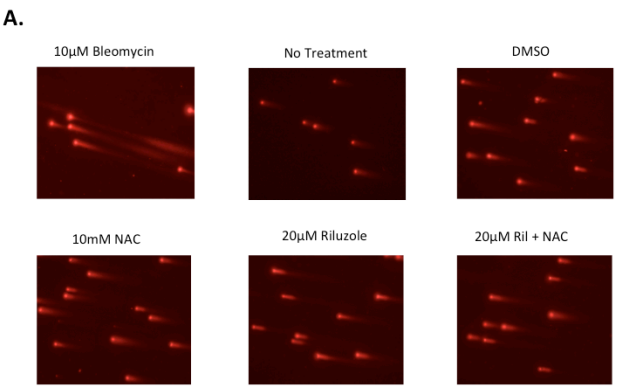

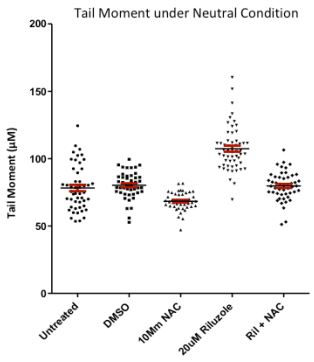

Figure 14. Neutral condition comet assay images after 48-hour riluzole treatment (A) and tail moment comparison across treatments (B). Double-stranded DNA breaks induced by riluzole was observed using the neutral COMET assay. Cells were serum starved for 48hours in 60mm tissue culture plates. Vehicle (0.1% DMSO) or riluzole(20μM) was given 24hours later with or without NAC (10mM) and cells were embedded in 1% agarose on a COMET slide at 48hour time point. DNA was stained using propidium iodide diluted to 1:100. Images were taken at 10X magnification using a confocal fluorescent microscope (A). Individual tail moments were calculated by measuring the radii and the tail length of individual cells and adding half the radius to half the tail lengths. Graph was generated using Graphpad Prism 6 (B).

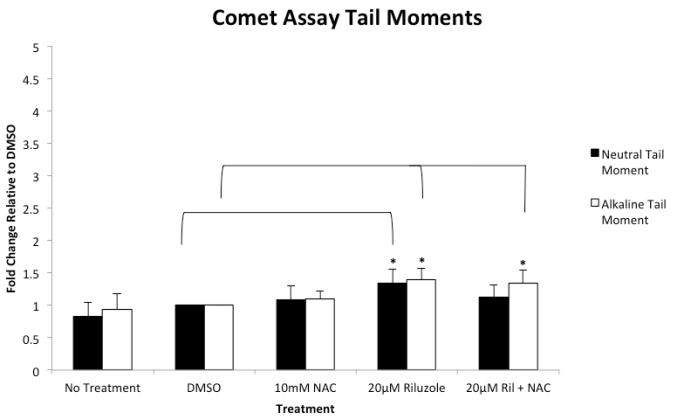

Figure 15. Comparison of average tail moments between neutral and alkaline condition comet assay after 48-hour riluzole treatment.
Tail moments from neutral and alkaline conditioned COMET assays were averaged and normalized to DMSO treated cells. Data were presented as mean tail moment induction relative to vehicle treatment (0.1% DMSO) +/- SEM (n=3 for alkaline condition and n=4 for neutral condition). An unstack one-way ANOVA analysis gives a $P<0.05$ for mean tail moments within both conditions. A student T test between riluzole only treatment and riluzole with NAC treat gives a p value of 0.18463 for the neutral condition and a p of 0.76747 for the alkaline condition. An asterisk (*) indicates statistical significance in a compare means T test compared to vehicle group.

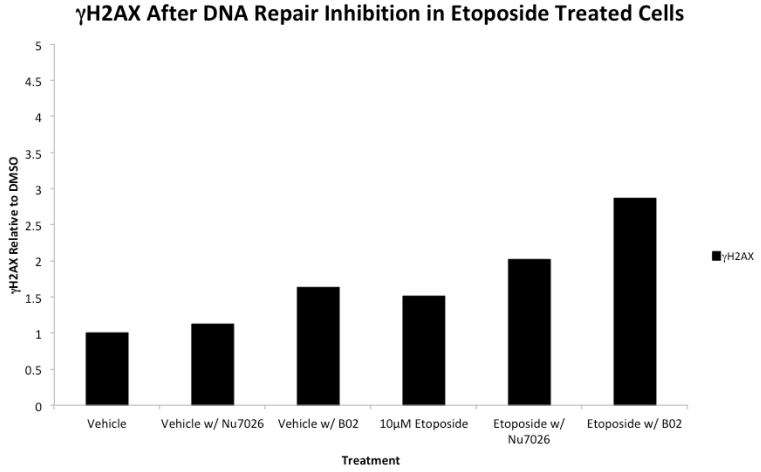

Figure 16. Induction of γH2AX by etoposide after DNA Repair inhibition.
Cells were serum starved for 48hours prior to being plated in a 12 well plate. At 24 hours later the cells were pretreated with DNA repair inhibitor Nu7026 (10μM) or B02 (10μM) for 6hours, the inhibitors were removed and etoposide (10μM) was added. After 24hour treatment cells were fixed in 70% methanol prior to immunostaining for γH2AX.

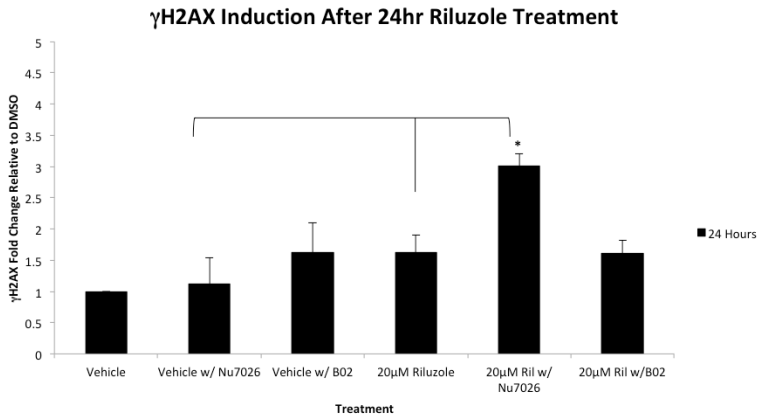

Figure 17. Induction of γH2AX by 24-hour riluzole treatment after inhibition of DNA repair enzymes.
Cells were serum starved for 48hours prior to being plated in a 12 well plate. At 24 hours later the cells were pretreated with DNA repair enzyme inhibitor Nu7026 (10μM) or B02 (10μM) for 6hours. After pretreatment, the inhibitors were removed, vehicle (0.1% DMSO) or riluzole (20μM) was add. After 24hour treatment cells, were fixed in 70% methanol prior to immunostaining for γH2AX. Data were presented as mean γH2AX fold change relative to vehicle (0.1% DMSO) treatment +/- SEM (n=3). A one-way unstacked ANOVA analysis with post-hoc bonferroni correction gives $p<0.05$, only in cells pretreated with NHEJ inhibitor, Nu7026. * indicates significance when comparing means of γH2AX levels in cells treated with riluzole plus Nu7026 to riluzole only or vehicle (DMSO) plus Nu7026.

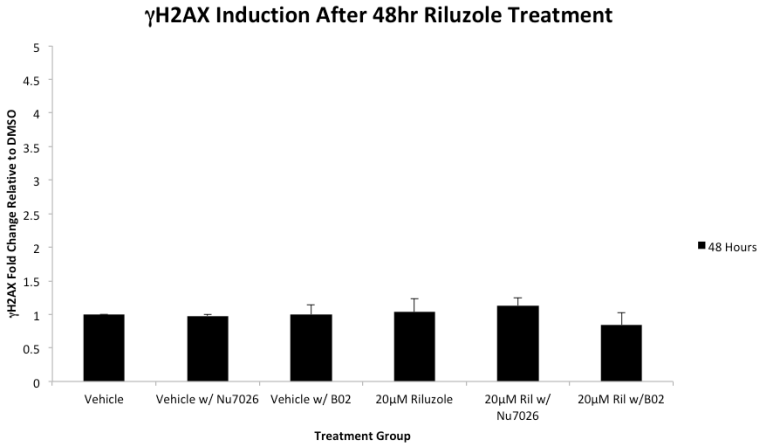

Figure 18. Induction of γH2AX by 48-hour riluzole treatment after DNA repair inhibition.
Cells were serum starved for 48hours prior to being plated in a 12 well plate. 24 hours later the cells were pretreated with DNA repair inhibitor Nu7026 (10μM) or B02 (10μM) for 6hours. After pretreatment, the inhibitors were removed and treatments were added: no treatment and vehicle (0.1% DMSO) and riluzole (20μM). After 48hour treatment, cells were fixed in 70% methanol prior to immunostaining for γH2AX. Data were presented as mean γH2AX fold change relative to vehicle (0.1% DMSO) treatment +/- SEM (n=3).

REFERENCES

Alagpulinsa, D. A., Ayyadevara, S., and Shmookler Reis, R. J. (2014). A Small-Molecule Inhibitor of RAD51 Reduces Homologous Recombination and Sensitizes Multiple Myeloma Cells to Doxorubicin. *Frontiers in Oncology* **4**, 289, 10.3389/fonc.2014.00289.

Anantha, R. W., Sokolova, E., and Borowiec, J. A. (2008). RPA phosphorylation facilitates mitotic exit in response to mitotic DNA damage. *Proceedings of the National Academy of Sciences of the United States of America* **105**(35), 12903-12908.

Banda, M., Speyer, C. L., Semma, S. N., Osuala, K. O., Kounalakis, N., Torres Torres, K. E., Barnard, N. J., Kim, H. J., Sloane, B. F., Miller, F. R., Goydos, J. S., and Gorski, D. H. (2014). Metabotropic glutamate receptor-1 contributes to progression in triple negative breast cancer. *PloS one* **9**(1), e81126, 10.1371/journal.pone.0081126.

Barzilai, A., and Yamamoto, K. (2004). DNA damage responses to oxidative stress. *DNA repair* **3**(8-9), 1109-15, 10.1016/j.dnarep.2004.03.002.

Baskar, R., Lee, K. A., Yeo, R., and Yeoh, K.-W. (2012). Cancer and radiation therapy: current advances and future directions. *Int J Med Sci* **9**(3), 193-199.

Bertrand, R. L. (2017). Iron accumulation, glutathione depletion, and lipid peroxidation must occur simultaneously during ferroptosis and are mutually amplifying events. *Medical hypotheses* **101**, 69-74, 10.1016/j.mehy.2017.02.017.

Bliss, T. V., and Collingridge, G. L. (1993). A synaptic model of memory: long-term potentiation in the hippocampus. *Nature* **361**(6407), 31-39.

Burden, D. A., and Osheroff, N. (1998). Mechanism of action of eukaryotic topoisomerase II and drugs targeted to the enzyme. *Biochim Biophys Acta* **1400**(1-3), 139-54.

Burger, M., Burger, J. A., Hoch, R. C., Oades, Z., Takamori, H., and Schraufstatter, I. U. (1999). Point mutation causing constitutive signaling of CXCR2 leads to transforming activity similar to Kaposi's sarcoma herpesvirus-G protein-coupled receptor. *Journal of immunology (Baltimore, Md. : 1950)* **163**(4), 2017-22.

Cerchia, C., and Lavecchia, A. (2017). Small Molecule Drugs and Targeted Therapy for Melanoma: Current Strategies and Future Directions. *Current medicinal chemistry* **24**(21), 2312-2344, 10.2174/0929867324666170414163937.

Chang, H. J., Yoo, B. C., Lim, S. B., Jeong, S. Y., Kim, W. H., and Park, J. G. (2005). Metabotropic glutamate receptor 4 expression in colorectal carcinoma and its prognostic significance. *CLINICAL CANCER RESEARCH* **11**(9), 3288-3295. First published on CLINICAL CANCER RESEARCH.

Chappell, W. H., Steelman, L. S., Long, J. M., Kempf, R. C., Abrams, S. L., Franklin, R. A., Basecke, J., Stivala, F., Donia, M., Fagone, P., Malaponte, G., Mazzarino, M. C., Nicoletti, F., Libra, M., Maksimovic-Ivanic, D., Mijatovic, S., Montalto, G., Cervello, M., Laidler, P., Milella, M., Tafuri, A., Bonati, A., Evangelisti, C., Cocco, L., Martelli, A. M., and McCubrey, J. A. (2011). Ras/Raf/MEK/ERK and PI3K/PTEN/Akt/mTOR inhibitors: rationale and importance to inhibiting these pathways in human health. *Oncotarget* **2**(3), 135-64, 10.18632/oncotarget.240.

Chintala, S., Li, W., Lamoreux, M. L., Ito, S., Wakamatsu, K., Sviderskaya, E. V., Bennett, D. C., Park, Y. M., Gahl, W. A., Huizing, M., Spritz, R. A., Ben, S., Novak, E. K., Tan, J., and Swank, R. T. (2005). Slc7a11 gene controls production of pheomelanin pigment and proliferation of cultured cells. *Proc Natl Acad Sci U S A* **102**(31), 10964-9, 10.1073/pnas.0502856102.

de Araújo, É. S. S., Pramio, D. T., and Krepischi, A. C. V. (2016). Chapter 7 - Role of CDKN2A Mutations and Other Relevant Genes in Melanoma Predisposition A2 - Hayat, M.A. In *Brain Metastases from Primary Tumors, Volume 3* (doi: https://doi.org/10.1016/B978-0-12-803508-5.00007-X, pp. 101-117. Academic Press, San Diego.

Dorr, R. T. (1992). Bleomycin pharmacology: mechanism of action and resistance, and clinical pharmacokinetics. *Seminars in oncology* **19**(2 Suppl 5), 3-8.

Gelb, T., Pshenichkin, S., Rodriguez, O. C., Hathaway, H. A., Grajkowska, E., DiRaddo, J. O., Wroblewska, B., Yasuda, R. P., Albanese, C., Wolfe, B. B., and Wroblewski, J. T. (2015). Metabotropic glutamate receptor 1 acts as a dependence receptor creating a requirement for glutamate to sustain the viability and growth of human melanomas. *Oncogene* **34**(21), 2711-20. First published on Oncogene, 10.1038/onc.2014.231.

Guo, L., Zhang, H., and Chen, B. (2017). Nivolumab as Programmed Death-1 (PD-1) Inhibitor for Targeted Immunotherapy in Tumor. *Journal of Cancer* **8**(3), 410-416, 10.7150/jca.17144.

Ha, L., Merlino, G., and Sviderskaya, E. V. (2008). Melanomagenesis: overcoming the barrier of melanocyte senescence. *Cell Cycle* **7**(13), 1944-8, 10.4161/cc.7.13.6230.

Hardiman, O., Al-Chalabi, A., Chio, A., Corr, E. M., Logroscino, G., Robberecht, W., Shaw, P. J., Simmons, Z., and van den Berg, L. H. (2017). Amyotrophic lateral sclerosis. *Nature Reviews Disease Primers* **3**, 17071, 10.1038/nrdp.2017.71.

Jakel, S., and Dimou, L. (2017). Glial Cells and Their Function in the Adult Brain: A Journey through the History of Their Ablation. *Frontiers in cellular neuroscience* **11**, 24, 10.3389/fncel.2017.00024.

Jansson, L. C., and Akerman, K. E. (2014). The role of glutamate and its receptors in the proliferation, migration, differentiation and survival of neural progenitor cells. *JOURNAL OF NEURAL TRANSMISSION* **121**(8), 819-836. First published on JOURNAL OF NEURAL TRANSMISSION.

Jasin, M., and Rothstein, R. (2013). Repair of Strand Breaks by Homologous Recombination. *Cold Spring Harbor perspectives in biology* **5**(11), a012740, 10.1101/cshperspect.a012740.

Jiang, L., Kon, N., Li, T., Wang, S. J., Su, T., Hibshoosh, H., Baer, R., and Gu, W. (2015). Ferroptosis as a p53-mediated activity during tumour suppression. *Nature* **520**(7545), 57-62, 10.1038/nature14344.

Julio-Pieper, M., Flor, P. J., Dinan, T. G., and Cryan, J. F. (2011). Exciting times beyond the brain: metabotropic glutamate receptors in peripheral and non-neural tissues. *Pharmacological reviews* **63**(1), 35-58.

Khan, A. J., Wall, B., Ahlawat, S., Green, C., Schiff, D., Mehnert, J. M., Goydos, J. S., Chen, S., and Haffty, B. G. (2011). Riluzole enhances ionizing radiation-induced cytotoxicity in human melanoma cells that ectopically express metabotropic glutamate receptor 1 in vitro and in vivo. *Clin Cancer Res* **17**(7), 1807-14. First published on Clin Cancer Res, 10.1158/1078-0432.ccr-10-1276.

Kondo, N., Takahashi, A., Ono, K., and Ohnishi, T. (2010). DNA damage induced by alkylating agents and repair pathways. *Journal of nucleic acids* **2010**, 543531, 10.4061/2010/543531.

Krokan, H. E., and Bjoras, M. (2013). Base excision repair. *Cold Spring Harbor perspectives in biology* **5**(4), a012583, 10.1101/cshperspect.a012583.

Kuo, L. J., and Yang, L. X. (2008). Gamma-H2AX - a novel biomarker for DNA double-strand breaks. *In vivo (Athens, Greece)* **22**(3), 305-9.

Le, M. N., Chan, J. L., Rosenberg, S. A., Nabatian, A. S., Merrigan, K. T., Cohen-Solal, K. A., and Goydos, J. S. (2010). The glutamate release inhibitor Riluzole decreases migration, invasion, and proliferation of melanoma cells. *J Invest Dermatol* **130**(9), 2240-9. First published on J Invest Dermatol, 10.1038/jid.2010.126.

Leger, A. J., Covic, L., and Kuliopulos, A. (2006). Protease-activated receptors in cardiovascular diseases. *Circulation* **114**(10), 1070-7, 10.1161/circulationaha.105.574830.

Lieber, M. R. (2010). The Mechanism of Double-Strand DNA Break Repair by the Nonhomologous DNA End Joining Pathway. *Annual review of biochemistry* **79**, 181-211, 10.1146/annurev.biochem.052308.093131.

Lipson, E. J., and Drake, C. G. (2011). Ipilimumab: an anti-CTLA-4 antibody for metastatic melanoma. *Clin Cancer Res* **17**(22), 6958-62, 10.1158/1078-0432.Ccr-11-1595.

Lüscher, C., and Huber, K. M. (2010). Group 1 mGluR-dependent synaptic long-term depression: mechanisms and implications for circuitry and disease. *Neuron* **65**(4), 445-459.

Luyt, K., Varadi, A., Halfpenny, C. A., Scolding, N. J., and Molnar, E. (2004). Metabotropic glutamate receptors are expressed in adult human glial progenitor cells. *Biochemical and Biophysical Research Communications* **319**, 120-129. First published on Biochemical and Biophysical Research Communications, 10.1016/j.bbrc.2004.04.158.

Mao, Z., Bozzella, M., Seluanov, A., and Gorbunova, V. (2008). DNA repair by nonhomologous end joining and homologous recombination during cell cycle in human cells. *Cell Cycle* **7**(18), 2902-2906, 10.4161/cc.7.18.6679.

Martin, D., Thompson, M. A., and Nadler, J. V. (1993). The neuroprotective agent riluzole inhibits release of glutamate and aspartate from slices of hippocampal area CA1. *European journal of pharmacology* **250**(3), 473-476.

Martino, J. J., Wall, B. A., Mastrantoni, E., Wilimczyk, B. J., La Cava, S. N., Degenhardt, K., White, E., and Chen, S. (2013). Metabotropic glutamate receptor 1 (Grm1) is an oncogene in epithelial cells. *Oncogene* **32**(37), 4366-76. First published on Oncogene, 10.1038/onc.2012.471.

Mehnert, J. M., Silk, A. W., Lee, J. H., Dudek, L., Jeong, B. S., Li, J., Schenkel, J. M., Sadimin, E., Kane, M., Lin, H., Shih, W. J., Zloza, A., Chen, S., and Goydos, J. S.

(2018). A phase II trial of riluzole, an antagonist of metabotropic glutamate receptor 1 (GRM1) signaling, in patients with advanced melanoma. *Pigment Cell Melanoma Res* **31**(4), 534-540, 10.1111/pcmr.12694.

Mehta, A., Prabhakar, M., Kumar, P., Deshmukh, R., and Sharma, P. L. (2013). Excitotoxicity: Bridge to various triggers in neurodegenerative disorders. *European Journal of Pharmacology* **698**(1–3), 6-18, http://dx.doi.org/10.1016/j.ejphar.2012.10.032.

Meister, A. (1995). [1] Glutathione metabolism. In *Methods in Enzymology* (Vol. 251, pp. 3-7. Academic Press.

Meldrum, B. S. (2000). Glutamate as a neurotransmitter in the brain: review of physiology and pathology. *The Journal of nutrition* **130**(4S Suppl), 1007s-15s, 10.1093/jn/130.4.1007S.

Menard, C., and Quirion, R. (2012). Group 1 metabotropic glutamate receptor function and its regulation of learning and memory in the aging brain. *Front Pharmacol* **3**, 182. First published on Front Pharmacol, 10.3389/fphar.2012.00182.

Namkoong, J., Shin, S. S., Lee, H. J., Marin, Y. E., Wall, B. A., Goydos, J. S., and Chen, S. (2007). Metabotropic glutamate receptor 1 and glutamate signaling in human melanoma. *Cancer Res* **67**(5), 2298-305, 10.1158/0008-5472.can-06-3665.

Nazarian, R., Shi, H., Wang, Q., Kong, X., Koya, R. C., Lee, H., Chen, Z., Lee, M. K., Attar, N., Sazegar, H., Chodon, T., Nelson, S. F., McArthur, G., Sosman, J. A., Ribas, A., and Lo, R. S. (2010). Melanomas acquire resistance to B-RAF(V600E) inhibition by RTK or N-RAS upregulation. *Nature* **468**(7326), 973-7, 10.1038/nature09626.

Niswender, C. M., and Conn, P. J. (2010). Metabotropic Glutamate Receptors: Physiology, Pharmacology, and Disease. *Annual review of pharmacology and toxicology* **50**, 295-322, 10.1146/annurev.pharmtox.011008.145533.

Ohtani, Y., Harada, T., Funasaka, Y., Nakao, K., Takahara, C., Abdel-Daim, M., Sakai, N., Saito, N., Nishigori, C., and Aiba, A. (2008). Metabotropic glutamate receptor subtype-1 is essential for in vivo growth of melanoma. *Oncogene* **27**, 7162, 10.1038/onc.2008.329.

Pollock, P. M., Cohen-Solal, K., Sood, R., Namkoong, J., Martino, J. J., Koganti, A., Zhu, H., Robbins, C., Makalowska, I., and Shin, S.-S. (2003). Melanoma mouse model implicates metabotropic glutamate signaling in melanocytic neoplasia. *Nature genetics* **34**(1), 108-112.

Reardon, J. T., and Sancar, A. (2005). Nucleotide Excision Repair. In *Progress in Nucleic Acid Research and Molecular Biology* (Vol. 79, pp. 183-235. Academic Press.

Schoepp, D. D. (2001). Unveiling the Functions of Presynaptic Metabotropic Glutamate Receptors in the Central Nervous System. *Journal of Pharmacology and Experimental Therapeutics* **299**(1), 12-20. First published on Journal of Pharmacology and Experimental Therapeutics.

Schonwasser, D. C., Marais, R. M., Marshall, C. J., and Parker, P. J. (1998). Activation of the mitogen-activated protein kinase/extracellular signal-regulated kinase pathway by conventional, novel, and atypical protein kinase C isotypes. *Mol Cell Biol* **18**(2), 790-8.

Shin, S. S., Namkoong, J., Wall, B. A., Gleason, R., Lee, H. J., and Chen, S. (2008). Oncogenic activities of metabotropic glutamate receptor 1 (Grm1) in melanocyte transformation. *Pigment Cell Melanoma Res* **21**(3), 368-78. First published on Pigment Cell Melanoma Res, 10.1111/j.1755-148X.2008.00452.x.

Siegel, R. L., Miller, K. D., and Jemal, A. (2018). Cancer statistics, 2018. *CA Cancer J Clin* **68**(1), 7-30, 10.3322/caac.21442.

Swenberg, J. A., Lu, K., Moeller, B. C., Gao, L., Upton, P. B., Nakamura, J., and Starr, T. B. (2011). Endogenous versus exogenous DNA adducts: their role in carcinogenesis, epidemiology, and risk assessment. *Toxicological sciences : an official journal of the Society of Toxicology* **120 Suppl 1**, S130-45, 10.1093/toxsci/kfq371.

Taylor, S. J., Chae, H. Z., Rhee, S. G., and Exton, J. H. (1991). Activation of the β1 isozyme of phospholipase C by α subunits of the Gq class of G proteins. *Nature* **350**, 516, 10.1038/350516a0.

van Zandwijk, N. (1995). N-acetylcysteine (NAC) and glutathione (GSH): antioxidant and chemopreventive properties, with special reference to lung cancer. *Journal of cellular biochemistry. Supplement* **22**, 24-32.

Vernon, A. C., Zbarsky, V., Datla, K. P., Croucher, M. J., and Dexter, D. T. (2007). Subtype selective antagonism of substantia nigra pars compacta Group I metabotropic glutamate receptors protects the nigrostriatal system against 6‐hydroxydopamine toxicity in vivo. *Journal of neurochemistry* **103**(3), 1075-1091.

Veuger, S. J., Curtin, N. J., Richardson, C. J., Smith, G. C. M., and Durkacz, B. W. (2003). Radiosensitization and DNA Repair Inhibition by the Combined Use of Novel Inhibitors of DNA-dependent Protein Kinase and Poly(ADP-Ribose) Polymerase-1. *Cancer Research* **63**(18), 6008.

Wall, B. A., Wangari-Talbot, J., Shin, S. S., Schiff, D., Sierra, J., Yu, L. J., Khan, A., Haffty, B., Goydos, J. S., and Chen, S. (2014). Disruption of GRM1-mediated signalling using riluzole results in DNA damage in melanoma cells. *Pigment Cell Melanoma Res* **27**(2), 263-74. First published on Pigment Cell Melanoma Res, 10.1111/pcmr.12207.

Wangari-Talbot, J., Wall, B. A., Goydos, J. S., and Chen, S. (2012a). Functional effects of GRM1 suppression in human melanoma cells. *Molecular cancer research : MCR* **10**(11), 1440-50, 10.1158/1541-7786.Mcr-12-0158.

Wangari-Talbot, J., Wall, B. A., Goydos, J. S., and Chen, S. (2012b). Functional effects of GRM1 suppression in human melanoma cells. *Molecular Cancer Research* **10**(11), 1440-1450.

Ward, J. F. (1988). DNA Damage Produced by Ionizing Radiation in Mammalian Cells: Identities, Mechanisms of Formation, and Reparability. In *Progress in Nucleic Acid Research and Molecular Biology* (W. E. Cohn, and K. Moldave, Eds.), Vol. 35, pp. 95-125. Academic Press.

Wolchok, J. D., Hodi, F. S., Weber, J. S., Allison, J. P., Urba, W. J., Robert, C., O'Day, S. J., Hoos, A., Humphrey, R., Berman, D. M., Lonberg, N., and Korman, A. J. (2013). Development of ipilimumab: a novel immunotherapeutic approach for the treatment of advanced melanoma. *Annals of the New York Academy of Sciences* **1291**, 1-13, 10.1111/nyas.12180.

Wu, Y. L., Wang, N. N., Gu, L., Yang, H. M., Xia, N., and Zhang, H. (2012). The suppressive effect of metabotropic glutamate receptor 5 (mGlu5) inhibition on hepatocarcinogenesis. *Biochimie* **94**(11), 2366-75. First published on Biochimie, 10.1016/j.biochi.2012.06.006.

Yin, Z., Ivanov, V. N., Habelhah, H., Tew, K., and Ronai, Z. e. (2000). Glutathione S-transferase p elicits protection against H2O2-induced cell death via coordinated regulation of stress kinases. *Cancer research* **60**(15), 4053-4057.

Yip, D., Le, M. N., Chan, J. L., Lee, J. H., Mehnert, J. A., Yudd, A., Kempf, J., Shih, W. J., Chen, S., and Goydos, J. S. (2009). A phase 0 trial of riluzole in patients with resectable stage III and IV melanoma. *Clin Cancer Res* **15**(11), 3896-902. First published on Clin Cancer Res, 10.1158/1078-0432.ccr-08-3303.

Young, D., Waitches, G., Birchmeier, C., Fasano, O., and Wigler, M. (1986). Isolation and characterization of a new cellular oncogene encoding a protein with multiple potential transmembrane domains. *Cell* **45**(5), 711-9.

Yu, L. J., Wall, B. A., Wangari-Talbot, J., and Chen, S. (2016). Metabotropic glutamate receptors in cancer. *Neuropharmacology* doi: 10.1016/j.neuropharm.2016.02.011. First published on Neuropharmacology, 10.1016/j.neuropharm.2016.02.011.

Zhang, C., Yuan, X. R., Li, H. Y., Zhao, Z. J., Liao, Y. W., Wang, X. Y., Su, J., Sang, S. S., and Liu, Q. (2015). Anti-cancer effect of metabotropic glutamate receptor 1 inhibition in human glioma U87 cells: involvement of PI3K/Akt/mTOR pathway. *Cellular physiology and biochemistry : international journal of experimental cellular physiology, biochemistry, and pharmacology* **35**(2), 419-32, 10.1159/000369707.

Zhao, L., Jiao, Q., Yang, P., Chen, X., Zhang, J., Zhao, B., Zheng, P., and Liu, Y. (2011). Cellular and Molecular Neuroscience: Metabotropic glutamate receptor 5 promotes proliferation of human neural stem/progenitor cells with activation of mitogen-activated protein kinases signaling pathway in vitro. *Neuroscience* **192**, 185-194. First published on Neuroscience, 10.1016/j.neuroscience.2011.06.044.